

# Efficient and Stable Schemes for the Magnetohydrodynamic Potential Model

Guo-Dong Zhang<sup>1</sup> and Xiaofeng Yang<sup>2,\*</sup>

<sup>1</sup> School of Mathematics and Information Sciences, Yantai University, Yantai, 264005, Shandong, P.R. China.

<sup>2</sup> Department of Mathematics, University of South Carolina, Columbia, SC, 29208, USA.

Received 20 June 2020; Accepted (in revised version) 19 January 2021

---

**Abstract.** In this paper, we consider the numerical approximations of a magnetohydrodynamic potential model that was developed in [15]. Several decoupled, linear, unconditionally energy stable schemes are developed by combining some subtle implicit-explicit treatments for nonlinear coupling terms and the projection-type method for the Navier-Stokes equations. The divergence-free condition for the magnetic field is preserved in the fully-discrete level. We further establish the well-posedness and unconditional energy stabilities of the proposed schemes and present a series of numerical examples in 3D, including accuracy/stability tests, benchmark simulations of driven cavity flow and hydromagnetic Kelvin-Helmholtz instability.

**AMS subject classifications:** 65M60

**Key words:** Potential MHD, linear, decoupled, energy stability, second-order, projection method.

---

## 1 Introduction

Magnetohydrodynamic (MHD) system describes the dynamic behaviors of an electrically conducting fluid under the influence of an external magnetic field. It occurs in geophysics, astrophysics, fusion reactor blankets, and confinement for controlled thermonuclear fusion, see [11, 26, 30]. The model involves multi-physics, thus the governing equations couple the Navier-Stokes equations for hydrodynamics and Maxwell's equations for electromagnetism. The two equations are coupled by the Lorentz force, which governs the effect of a magnetic field on fluid flow, and the appearance of the fluid velocity in Ohm's law, which accounts for the influence of hydrodynamics on the electric current. Concerning the corresponding extensive theoretical/numerical studies including the modeling and PDE analysis of the MHD system, we refer to [1–3, 9, 13, 14, 17–19, 21, 24, 29, 32, 33, 39] and the references therein.

---

\*Corresponding author. *Email addresses:* gdzhang@ytu.edu.cn (G.-D. Zhang), xfyang@math.sc.edu (X. Yang)

The magnetic field  $\mathbf{B}$  in MHD models usually satisfies the divergence-free condition ( $\nabla \cdot \mathbf{B} = 0$ ) that is a precise physical law in electro-magnetics which implies that there is no source of the magnetic field in the domain. It is very important to preserve this condition in the discrete level since it has been shown that even tiny perturbations to this condition may lead to large errors in numerical simulations, see [5, 8, 22, 38]. Recently, a novel, so-called MHD potential model is developed in [15], in which a magnetic potential vector field  $A$  is introduced and the magnetic field is then defined as its rotation, i.e.,  $\mathbf{B} = \nabla \times A$ . In this way, the numerical solution of the magnetic field  $\mathbf{B}_h$  can be recovered automatically by  $\mathbf{B}_h = \nabla \times A_h$  which in turn ensures the exact divergence-free condition. Meanwhile, to solve the model, two numerical schemes (one linear and one nonlinear) based on the Crank-Nicolson methods were developed in [15]. However, the algorithms are coupled type which implies that the fluid velocity, the magnetic potential, and the pressure are all coupled together at each time step.

Hence, in this paper, we aim to develop some more efficient numerical schemes to solve the MHD potential model developed in [15]. We are particularly interested in designing energy stable schemes, in the sense that the discrete energy dissipation laws may hold. In the meantime, while keeping the energy stable feature, we prefer to develop schemes that are easy-to-implement which is referred to linear and decoupled in comparison with its counterparts: nonlinear and coupled. To this end, the main challenging issue that is needed to overcome is to develop suitable temporal discretizations for a large number of nonlinear and coupling terms, including (i) the coupling between the velocity and pressure in the fluid momentum equation; (ii) the nonlinear coupling between the magnetic potential and the fluid velocity field through the convection; and (iii) the nonlinear coupling between the fluid velocity and the magnetic potential through the Lorentz force. We expect to construct a time discretization scheme which (a) is unconditionally stable; (b) satisfies a discrete energy law; and (c) leads to decoupled equations to solve at each time step. This is by no means an easy task due to the highly nonlinear coupling nature appears in the MHD potential model.

The rest of the paper is organized as follows. In Section 2, we present the MHD potential model and derive the associated energy dissipation law. In Section 3, we present a first-order scheme and two second-order schemes and prove their well-posedness and unconditional energy stabilities. In Section 4, a series of 3D numerical examples are implemented including accuracy/stability tests, benchmark simulations of driven cavity flow and hydromagnetic Kelvin-Helmholtz instability to demonstrate the stability and accuracy of the schemes. Finally, some concluding remarks are given in Section 5.

## 2 The potential MHD model and its energy law

In this section, we present the magnetic potential MHD model and demonstrate its energy dissipation law. Throughout this paper, we consider the incompressible MHD problem in a bounded Lipschitz domain  $\Omega \subset \mathbb{R}^3$  with the boundary  $\partial\Omega$ . The magnetic poten-

tial MHD model [15] can be written in a dimensionless form as follows,

$$\mathbf{u}_t - \nu \Delta \mathbf{u} + (\mathbf{u} \cdot \nabla) \mathbf{u} + \nabla p + s(\mathbf{A}_t + \nabla \times \mathbf{A} \times \mathbf{u}) \times \nabla \times \mathbf{A} = 0 \quad \text{in } \Omega, \quad (2.1)$$

$$\nabla \cdot \mathbf{u} = 0 \quad \text{in } \Omega, \quad (2.2)$$

$$\mathbf{A}_t + \eta \nabla \times \nabla \times \mathbf{A} + \nabla \times \mathbf{A} \times \mathbf{u} = 0 \quad \text{in } \Omega, \quad (2.3)$$

$$\mathbf{u}(0) = \mathbf{u}^0, \quad \mathbf{A}(0) = \mathbf{A}^0 \quad \text{in } \Omega, \quad (2.4)$$

$$\mathbf{u} = 0, \quad \mathbf{A} \times \mathbf{n} = 0 \quad \text{on } \partial\Omega, \quad (2.5)$$

where  $\mathbf{u}$  denotes the velocity field,  $p$  is the pressure,  $\mathbf{n}$  is the outward normal, and  $\mathbf{A}$  is the magnetic vector potential. Note the magnetic field  $\mathbf{B}$  is defined as  $\mathbf{B} = \nabla \times \mathbf{A}$  hence  $\nabla \cdot \mathbf{B} = 0$  naturally. In this paper, all of the bold-lettered symbols represent vectors.

For the physical parameters,  $\nu^{-1} = R_e$  (fluid Reynolds number),  $\eta^{-1} = R_m$  (magnetic Reynolds number), and  $s$  is the coupling coefficient, which are given by

$$R_e = \frac{UL}{\mu_f}, \quad R_m = \mu_m \sigma UL, \quad s = \frac{B^2}{\rho \mu_m U^2},$$

where  $U$  is the characteristic velocity,  $L$  is the characteristic length,  $\mu_f$  is the kinematic viscosity,  $\mu_m$  is the magnetic permeability,  $\sigma$  is the electric conductivity,  $B$  is the characteristic magnetic field, and  $\rho$  is the fluid density.

We define some notations of function spaces and norms. For two vector functions  $\mathbf{x}, \mathbf{y}$ , we denote the  $L^2$  inner product as  $(\mathbf{x}, \mathbf{y}) = \int_{\Omega} \mathbf{x} \cdot \mathbf{y} dx$  and  $L^2$  norm  $\|\mathbf{x}\|^2 = (\mathbf{x}, \mathbf{x})$ . For function setting for this MHD model, we also need the standard Sobolev spaces:

$$\mathbf{H}_0^1(\Omega) = \left\{ \boldsymbol{\phi} \in H^1(\Omega)^3 : \boldsymbol{\phi}|_{\partial\Omega} = 0 \right\},$$

$$L_0^2(\Omega) = \left\{ \phi \in L^2(\Omega) : \int_{\Omega} \phi dx = 0 \right\},$$

$$H_0(\text{curl}, \Omega) = \left\{ \mathbf{w} \in L^2(\Omega)^3, \nabla \times \mathbf{w} \in L^2(\Omega)^3 : \mathbf{n} \times \mathbf{w}|_{\partial\Omega} = 0 \right\},$$

and use  $\|\cdot\|_1$  for the norm in  $H^1(\Omega)^3$ ,  $\|\cdot\|_{\text{curl}}$  for the norm in  $H_0(\text{curl}, \Omega)$ . In  $\mathbf{H}_0^1(\Omega)$  space, there also holds the well-known Poincaré inequalities [10]

$$\|\mathbf{w}\|_1 \leq C_{\Omega} \|\nabla \mathbf{w}\|, \quad \mathbf{w} \in \mathbf{H}_0^1(\Omega). \quad (2.6)$$

The model (2.1)-(2.5) possesses the energy dissipation law. By taking the  $L^2$  inner product of (2.1) with  $\mathbf{u}$ , and of (2.3) with  $s\mathbf{A}_t$ , using  $(\mathbf{u} \cdot \nabla \mathbf{u}, \mathbf{u}) = 0$ ,  $\mathbf{u}|_{\partial\Omega} = 0$ ,  $\nabla \cdot \mathbf{u} = 0$  and integration by parts, we derive

$$\frac{1}{2} \frac{d}{dt} \|\mathbf{u}\|^2 + \nu \|\nabla \mathbf{u}\|^2 + s(\mathbf{A}_t + \nabla \times \mathbf{A} \times \mathbf{u}, \nabla \times \mathbf{A} \times \mathbf{u}) = 0, \quad (2.7)$$

and

$$\frac{1}{2} s \eta \frac{d}{dt} \|\nabla \times \mathbf{A}\|^2 + s(\mathbf{A}_t + \nabla \times \mathbf{A} \times \mathbf{u}, \mathbf{A}_t) = 0. \quad (2.8)$$

By taking the summations of (2.7) and (2.8), we arrive at

$$\frac{1}{2} \frac{d}{dt} \|\mathbf{u}\|^2 + \frac{1}{2} s \eta \frac{d}{dt} \|\nabla \times \mathbf{A}\|^2 + \nu \|\nabla \mathbf{u}\|^2 + s \|\mathbf{A}_t + \nabla \times \mathbf{A} \times \mathbf{u}\|^2 = 0,$$

which implies that

$$\frac{d}{dt} E(\mathbf{u}, \mathbf{A}) = -\nu \|\nabla \mathbf{u}\|^2 - s \|\mathbf{A}_t + \nabla \times \mathbf{A} \times \mathbf{u}\|^2, \quad (2.9)$$

where

$$E(\mathbf{u}, \mathbf{A}) = \frac{1}{2} \|\mathbf{u}\|^2 + \frac{1}{2} s \eta \|\nabla \times \mathbf{A}\|^2.$$

### 3 Numerical schemes

#### 3.1 First-order scheme

In this section, we propose the first-order scheme for solving the MHD system (2.1)-(2.5), and prove its well-posedness and unconditional energy stability. We first present time-marching scheme for (2.1)-(2.5) and then generalize it to be the fully-discrete version.

Let  $\delta t > 0$  denote the time step size and set  $t_n = n\delta t$  for  $0 < n < \lceil \frac{T}{\delta t} \rceil$  with the final time  $T$ . We denote  $d_t \psi^{n+1} = \frac{\psi^{n+1} - \psi^n}{\delta t}$  for a variable  $\psi$ .

The first-order time-marching semi-discrete scheme reads as follows.

Given the initial conditions  $(\mathbf{u}^0, \mathbf{A}^0), p^0 = 0$ , having computed  $(\mathbf{u}^n, \mathbf{A}^n, p^n)$  for  $n > 0$ , we update  $(\mathbf{u}^{n+1}, \mathbf{A}^{n+1}, p^{n+1})$  by the following steps.

*Step 1.* We solve  $\mathbf{A}^{n+1}$  from

$$\begin{cases} d_t \mathbf{A}^{n+1} + \eta \nabla \times \nabla \times \mathbf{A}^{n+1} + \nabla \times \mathbf{A}^n \times \mathbf{u}^n + s \nabla \times \mathbf{A}^n \times ((\mathbf{A}^{n+1} - \mathbf{A}^n) \times \nabla \times \mathbf{A}^n) = 0, \\ \mathbf{A}^{n+1} \times \mathbf{n}|_{\partial\Omega} = 0. \end{cases} \quad (3.1)$$

*Step 2.* We solve  $\tilde{\mathbf{u}}^{n+1}$  from

$$\begin{cases} \frac{\tilde{\mathbf{u}}^{n+1} - \mathbf{u}^n}{\delta t} - \nu \Delta \tilde{\mathbf{u}}^{n+1} + \mathbf{u}^n \nabla \tilde{\mathbf{u}}^{n+1} + \nabla p^n + s \nabla \times \mathbf{A}^n \times \tilde{\mathbf{u}}^{n+1} \times \nabla \times \mathbf{A}^n \\ \quad + s d_t \mathbf{A}^{n+1} \times \nabla \times \mathbf{A}^n = 0, \\ \tilde{\mathbf{u}}^{n+1}|_{\partial\Omega} = 0. \end{cases} \quad (3.2)$$

*Step 3.* We solve  $\mathbf{u}^{n+1}$  and  $p^{n+1}$  from

$$\begin{cases} \frac{\mathbf{u}^{n+1} - \tilde{\mathbf{u}}^{n+1}}{\delta t} + \nabla(p^{n+1} - p^n) = 0, \\ \nabla \cdot \mathbf{u}^{n+1} = 0, \\ \mathbf{u}^{n+1} \cdot \mathbf{n}|_{\partial\Omega} = 0. \end{cases} \quad (3.3)$$

**Remark 3.1.** In (3.1), we add a first-order stabilized term  $s\nabla \times A^n \times ((A^{n+1} - A^n) \times \nabla \times A^n)$  in the magnetic potential equation (3.1) (cf. the similar technique used for different models in [20, 34–36]). This term introduces some extra errors but plays an important role to ensure the unconditional energy stability (shown in Theorem 3.2). Besides, in (3.1)-(3.2), the subtle implicit and explicit combinations for the nonlinear and coupling terms are used to obtain the linear, fully-decoupled, and unconditionally energy stable algorithm.

**Remark 3.2.** By applying the divergence operator to the first equation of (3.3), we obtain

$$-\Delta p^{n+1} = -\frac{1}{\delta t} \nabla \cdot \tilde{\mathbf{u}}^{n+1} - \Delta p^n, \quad (3.4)$$

associated with the Neumann boundary conditions  $\partial_n(p^{n+1} - p^n)|_{\partial\Omega} = 0$ . Once  $p^{n+1}$  is obtained, we update  $\mathbf{u}^{n+1}$  from

$$\mathbf{u}^{n+1} = \tilde{\mathbf{u}}^{n+1} - \delta t \nabla(p^{n+1} - p^n).$$

Next, based on the semi-discrete scheme (3.1)-(3.3), we develop a fully-discrete scheme where the space is discretized by using the finite element method. To do so, we introduce some conforming finite element spaces:  $\mathbf{V}_h \subset \mathbf{H}_0^1(\Omega)$ ,  $Q_h \subset L_0^2(\Omega) \cap H^1(\Omega)$  which satisfy the so-called *inf-sup* condition, i.e., there exists a positive constant  $\beta$  such that

$$\beta \|q_h\| \leq \sup_{\mathbf{v}_h \in \mathbf{V}_h} \frac{(\nabla \cdot \mathbf{v}_h, q_h)}{\|\nabla \mathbf{v}_h\|}, \quad \forall q_h \in Q_h. \quad (3.5)$$

For the vector magnetic potential  $\mathbf{A}$ , we use  $H(\text{curl})$ -conforming Nédélec edge element space  $\mathbf{C}_h \subset H_0(\text{curl}; \Omega)$  to approximate the potential function  $\mathbf{A}$ . Hence, the finite element fully-discrete scheme reads as:

*Step 1.* Find  $\mathbf{A}_h^{n+1} \in \mathbf{C}_h$ , such that for  $\forall \boldsymbol{\phi}_h \in \mathbf{C}_h$ ,

$$\begin{aligned} & \left( \frac{\mathbf{A}_h^{n+1} - \mathbf{A}_h^n}{\delta t}, \boldsymbol{\phi}_h \right) + \eta (\nabla \times \mathbf{A}_h^{n+1}, \nabla \times \boldsymbol{\phi}_h) + (\nabla \times \mathbf{A}_h^n \times \mathbf{u}_h^n, \boldsymbol{\phi}_h) \\ & + s (\nabla \times \mathbf{A}_h^n \times (\mathbf{A}_h^{n+1} - \mathbf{A}_h^n), \nabla \times \mathbf{A}_h^n \times \boldsymbol{\phi}_h) = 0. \end{aligned} \quad (3.6)$$

*Step 2.* Find  $\tilde{\mathbf{u}}_h^{n+1} \in \mathbf{V}_h$  such that for  $\forall \mathbf{v}_h \in \mathbf{V}_h$ ,

$$\begin{aligned} & \left( \frac{\tilde{\mathbf{u}}_h^{n+1} - \mathbf{u}_h^n}{\delta t}, \mathbf{v}_h \right) + \nu (\nabla \tilde{\mathbf{u}}_h^{n+1}, \nabla \mathbf{v}_h) + b(\mathbf{u}_h^n, \tilde{\mathbf{u}}_h^{n+1}, \mathbf{v}_h) - (p_h^n, \nabla \cdot \mathbf{v}_h) \\ & + s (\nabla \times \mathbf{A}_h^n \times \tilde{\mathbf{u}}_h^{n+1}, \nabla \times \mathbf{A}_h^n \times \mathbf{v}_h) + s (d_t \mathbf{A}_h^{n+1} \times \nabla \times \mathbf{A}_h^n, \mathbf{v}_h) = 0. \end{aligned} \quad (3.7)$$

*Step 3.* Find  $p_h^{n+1} \in Q_h$  such that for  $\forall q_h \in Q_h$ ,

$$(\nabla p_h^{n+1}, \nabla q_h) = -\frac{1}{\delta t} (\nabla \cdot \tilde{\mathbf{u}}_h^{n+1}, q_h) + (\nabla p_h^n, \nabla q_h). \quad (3.8)$$

Step 4. We update  $\mathbf{u}_h^{n+1} \in \mathbf{V}_h + \nabla Q_h$  from

$$\mathbf{u}_h^{n+1} = \tilde{\mathbf{u}}_h^{n+1} - \delta t \nabla (p_h^{n+1} - p_h^n). \quad (3.9)$$

Several remarks are in order.

**Remark 3.3.** For the convective term in (3.7), we use the trilinear form as follows (cf. [37]),

$$b(\mathbf{u}, \mathbf{v}, \mathbf{w}) := \frac{1}{2}((\mathbf{u} \cdot \nabla) \mathbf{v}, \mathbf{w}) - \frac{1}{2}((\mathbf{u} \cdot \nabla) \mathbf{w}, \mathbf{v}).$$

Note when  $\mathbf{u} \in \mathbf{H}^1(\Omega), \mathbf{v}, \mathbf{w} \in \mathbf{H}_0^1(\Omega)$ , by using the integration by parts, we derive

$$b(\mathbf{u}, \mathbf{v}, \mathbf{w}) = ((\mathbf{u} \cdot \nabla) \mathbf{v}, \mathbf{w}) + \frac{1}{2}((\nabla \cdot \mathbf{u}) \mathbf{v}, \mathbf{w}).$$

Therefore, we obtain  $b(\mathbf{u}, \mathbf{u}, \mathbf{w}) = ((\mathbf{u} \cdot \nabla) \mathbf{u}, \mathbf{w})$  for the incompressible flow system since  $\nabla \cdot \mathbf{u} = 0$ .

**Remark 3.4.** The final velocity field  $\mathbf{u}_h^{n+1}$  satisfies the discrete divergence free condition. This can be deduced by taking the  $L^2$  inner product of (3.9) with  $\nabla q_h$ , we obtain

$$(\mathbf{u}_h^{n+1}, \nabla q_h) = -(\nabla \cdot \tilde{\mathbf{u}}_h^{n+1}, q_h) - \delta t (\nabla (p_h^{n+1} - p_h^n), \nabla q_h).$$

After combining with (3.8), we arrive at

$$(\mathbf{u}_h^{n+1}, \nabla q_h) = 0, \quad \forall q_h \in Q_h. \quad (3.10)$$

**Remark 3.5.** It is remarkable that (3.6) and (3.8) possess the symmetric positive definite (SPD) property. Hence, these two equations can be solved by preconditioned Conjugate Gradient (PCG) solver. However, (3.7) is not symmetric due to the skew symmetric term  $b(\mathbf{u}_h^n, \tilde{\mathbf{u}}_h^{n+1}, \mathbf{v}_h)$  which is implemented by using nonsymmetric solvers.

The well-posedness of the scheme (3.6)-(3.9) is demonstrated in the following theorem.

**Theorem 3.1.** *The scheme (3.6)-(3.9) admits a unique solution  $(\mathbf{A}_h^{n+1}, p_h^{n+1}, \mathbf{u}_h^{n+1})$  in  $\mathbf{C}_h \times Q_h \times \mathbf{V}_h$ .*

*Proof.* We define a bilinear form  $a_1(\cdot, \cdot) : \mathbf{C}_h \times \mathbf{C}_h \rightarrow \mathbb{R}$  by

$$a_1(\mathbf{A}, \boldsymbol{\phi}) = \frac{1}{\delta t}(\mathbf{A}, \boldsymbol{\phi}) + \eta(\nabla \times \mathbf{A}, \nabla \times \boldsymbol{\phi}) + s(\nabla \times \mathbf{A}_h^n \times \mathbf{A}, \nabla \times \mathbf{A}_h^n \times \boldsymbol{\phi}),$$

and a linear form  $L_1(\cdot) : \mathbf{C}_h \rightarrow \mathbb{R}$  by

$$L_1(\boldsymbol{\phi}) = \frac{1}{\delta t}(\mathbf{A}_h^n, \boldsymbol{\phi}) - (\nabla \times \mathbf{A}_h^n \times \mathbf{u}_h^n, \boldsymbol{\phi}) + s(\nabla \times \mathbf{A}_h^n \times \mathbf{A}_h^n, \nabla \times \mathbf{A}_h^n \times \boldsymbol{\phi}).$$

Then, the first step (3.6) can be expressed as: find  $A_h^{n+1} \in C_h$  such that for  $\forall \phi_h \in C_h$ ,

$$a_1(A_h^{n+1}, \phi_h) = L_1(\phi_h).$$

It can be verified that  $a_1(\cdot, \cdot)$  is bounded and coercive in  $C_h \times C_h$ :

$$\begin{aligned} a_1(A, \phi) &\leq \frac{1}{\delta t} \|A\| \|\phi\| + \eta \|\nabla \times A\| \|\nabla \times \phi\| + s \|\nabla \times A_h^n\|_{L^\infty} \|A\| \|\phi\| \\ &\leq C_1 \|A\|_{curl} \|\phi\|_{curl}, \end{aligned}$$

and

$$a_1(A, A) = \frac{1}{\delta t} \|A\|^2 + \eta \|\nabla \times A\|^2 + s \|\nabla \times A_h^n \times A\|^2 \geq \bar{C}_1 \|A\|_{curl}^2,$$

where  $C_1$  depends on  $\delta t, \eta, s, \|\nabla \times A_h^n\|_{L^\infty}$ , and  $\bar{C}_1$  depends on  $\delta t$  and  $\eta$ . Therefore, (3.6) admits a unique solution  $A_h^{n+1} \in C_h$  from the Lax-Milgram theorem.

In a similar way, we define a bilinear form  $a_2(\cdot, \cdot) : V_h \times V_h \rightarrow \mathbb{R}$  by

$$a_2(\mathbf{u}, \mathbf{v}) = \frac{1}{\delta t} (\mathbf{u}, \mathbf{v}) + \nu (\nabla \mathbf{u}, \nabla \mathbf{v}) + b(\mathbf{u}_h^n, \mathbf{u}, \mathbf{v}) + s (\nabla \times \mathbf{A}_h^n \times \mathbf{u}, \nabla \times \mathbf{A}_h^n \times \mathbf{v}),$$

and a linear form  $L_2(\cdot) : V_h \rightarrow \mathbb{R}$  by

$$L_2(\mathbf{v}) = \frac{1}{\delta t} (\mathbf{u}_h^n, \mathbf{v}) + (p_h^n, \nabla \cdot \mathbf{v}) - s (d_t \mathbf{A}_h^{n+1} \times \nabla \times \mathbf{A}_h^n, \mathbf{v}).$$

Then, the second step (3.7) can be written as: find  $\tilde{\mathbf{u}}_h^{n+1} \in V_h$  such that for  $\forall \mathbf{v}_h \in V_h$

$$a_2(\tilde{\mathbf{u}}_h^{n+1}, \mathbf{v}_h) = L_2(\mathbf{v}_h).$$

Using (2.6), we can verify  $a_2(\cdot, \cdot)$  also satisfies boundedness and coercivity in  $V_h \times V_h$ :

$$\begin{aligned} a_2(\mathbf{u}, \mathbf{v}) &\leq \frac{1}{\delta t} \|\mathbf{u}\| \|\mathbf{v}\| + \nu \|\nabla \mathbf{u}\| \|\nabla \mathbf{v}\| + \frac{1}{2} \|\mathbf{u}_h^n\|_{L^3} \|\nabla \mathbf{u}\| \|\mathbf{v}\|_{L^6} + \frac{1}{2} \|\mathbf{u}_h^n\|_{L^3} \|\nabla \mathbf{v}\| \|\mathbf{u}\|_{L^6} \\ &\quad + s \|\nabla \times \mathbf{A}_h^n\|_{L^3}^2 \|\mathbf{u}\|_{L^6} \|\mathbf{v}\|_{L^6} \\ &\leq \frac{1}{\delta t} \|\mathbf{u}\| \|\mathbf{v}\| + \nu \|\nabla \mathbf{u}\| \|\nabla \mathbf{v}\| + C_\Omega \|\mathbf{u}_h^n\|_{L^3} \|\mathbf{u}\|_1 \|\mathbf{v}\|_1 + s C_\Omega \|\nabla \times \mathbf{A}_h^n\|_{L^3}^2 \|\mathbf{u}\|_1 \|\mathbf{v}\|_1 \\ &\leq C_2 \|\mathbf{u}\|_1 \|\mathbf{v}\|_1, \end{aligned}$$

and

$$a_2(\mathbf{u}, \mathbf{u}) = \frac{1}{\delta t} \|\mathbf{u}\|^2 + \nu \|\nabla \mathbf{u}\|^2 + s \|\nabla \times \mathbf{A}_h^n \times \mathbf{u}\|^2 \geq \bar{C}_2 \|\mathbf{u}\|_1^2,$$

where  $C_2$  depends on  $\delta t, \nu, s, \Omega, \|\mathbf{u}_h^n\|_{L^3}, \|\nabla \times \mathbf{A}_h^n\|_{L^3}$ , and  $\bar{C}_2$  depends on  $\nu$  and  $\Omega$ . Thus, by Lax-Milgram theorem, we conclude (3.7) admits a unique solution  $\tilde{\mathbf{u}}_h^{n+1} \in V_h$ .

It is trivial to prove the third step (3.8) is also well-posed in  $Q_h$ , which completes the proof.  $\square$

There are two advantages in the scheme (3.6)-(3.9): *linear* and *fully-decoupled*. Namely, the scheme is totally linear and the magnetic potential  $A$ , pressure  $p$ , and velocity  $u$  can be solved independently at every time step. Moreover, the scheme (3.6)-(3.9) satisfies the energy dissipation law unconditionally in the discrete level, which is shown in the following theorem.

**Theorem 3.2.** *The scheme (3.6)-(3.9) is unconditionally energy stable in the sense that*

$$\begin{aligned} & \|u_h^{n+1}\|^2 + s\eta \|\nabla \times A_h^{n+1}\|^2 + \delta t^2 \|\nabla p_h^{n+1}\|^2 \\ & + 2\delta t\nu \|\nabla \tilde{u}_h^{n+1}\|^2 + 2\delta ts \|\mathcal{d}_t A_h^{n+1} + \nabla \times A_h^n \times \tilde{u}_h^{n+1}\|^2 \\ & \leq \|u_h^n\|^2 + s\eta \|\nabla \times A_h^n\|^2 + \delta t^2 \|\nabla p_h^n\|^2. \end{aligned} \quad (3.11)$$

*Proof.* Taking  $\phi_h = s\mathcal{d}_t A_h^{n+1}$  in (3.6), we derive

$$\begin{aligned} & s \|\mathcal{d}_t A_h^{n+1}\|^2 + \frac{s\eta}{2\delta t} (\|\nabla \times A_h^{n+1}\|^2 + \|\nabla \times A_h^{n+1} - \nabla \times A_h^n\|^2 - \|\nabla \times A_h^n\|^2) \\ & + s(\nabla \times A_h^n \times u_h^n, \mathcal{d}_t A_h^{n+1}) + s^2 \delta t \|\nabla \times A_h^n \times \mathcal{d}_t A_h^{n+1}\|^2 = 0. \end{aligned} \quad (3.12)$$

Taking  $\tilde{u}_h^{n+1}$  in (3.7), we get

$$\begin{aligned} & \frac{1}{2\delta t} (\|\tilde{u}_h^{n+1}\|^2 + \|\tilde{u}_h^{n+1} - u_h^n\|^2 - \|u_h^n\|^2) + \nu \|\nabla \tilde{u}_h^{n+1}\|^2 + (\nabla p_h^n, \tilde{u}_h^{n+1}) \\ & + s \|\nabla \times A_h^n \times \tilde{u}_h^{n+1}\|^2 + s(\mathcal{d}_t A_h^{n+1} \times \nabla \times A_h^n, \tilde{u}_h^{n+1}) = 0. \end{aligned} \quad (3.13)$$

We rewrite (3.9) as

$$\frac{1}{\delta t} u_h^{n+1} + \nabla p_h^{n+1} = \frac{1}{\delta t} \tilde{u}_h^{n+1} + \nabla p_h^n. \quad (3.14)$$

By taking the  $L^2$  inner product of (3.14) with itself on both sides, and using (3.10), we obtain

$$\frac{1}{2\delta t} \|u_h^{n+1}\|^2 - \frac{1}{2\delta t} \|\tilde{u}_h^{n+1}\|^2 + \frac{\delta t}{2} \|\nabla p_h^{n+1}\|^2 - \frac{\delta t}{2} \|\nabla p_h^n\|^2 = (\tilde{u}_h^{n+1}, \nabla p_h^n). \quad (3.15)$$

Then, by taking the summations of (3.12), (3.13) and (3.15), we obtain

$$\begin{aligned} & s \|\mathcal{d}_t A_h^{n+1}\|^2 + \frac{s\eta}{2\delta t} (\|\nabla \times A_h^{n+1}\|^2 + \|\nabla \times (A_h^{n+1} - A_h^n)\|^2 - \|\nabla \times A_h^n\|^2) \\ & + s^2 \delta t \|\nabla \times A_h^n \times \mathcal{d}_t A_h^{n+1}\|^2 + \frac{1}{2\delta t} (\|u_h^{n+1}\|^2 + \|\tilde{u}_h^{n+1} - u_h^n\|^2 - \|u_h^n\|^2) + \nu \|\nabla \tilde{u}_h^{n+1}\|^2 \\ & + \frac{\delta t}{2} \|\nabla p_h^{n+1}\|^2 - \frac{\delta t}{2} \|\nabla p_h^n\|^2 + s \|\nabla \times A_h^n \times \tilde{u}_h^{n+1}\|^2 \\ & + s(\nabla \times A_h^n \times u_h^n, \mathcal{d}_t A_h^{n+1}) + s(\nabla \times A_h^n \times \tilde{u}_h^{n+1}, \mathcal{d}_t A_h^{n+1}) = 0. \end{aligned} \quad (3.16)$$

To handle the last two terms in (3.16), we split  $s(\nabla \times \mathbf{A}_h^n \times \mathbf{u}_h^n, d_t \mathbf{A}_h^{n+1})$  as

$$s(\nabla \times \mathbf{A}_h^n \times \mathbf{u}_h^n, d_t \mathbf{A}_h^{n+1}) = s(\nabla \times \mathbf{A}_h^n \times (\mathbf{u}_h^n - \tilde{\mathbf{u}}_h^{n+1}), d_t \mathbf{A}_h^{n+1}) + s(\nabla \times \mathbf{A}_h^n \times \tilde{\mathbf{u}}_h^{n+1}, d_t \mathbf{A}_h^{n+1}).$$

Then, (3.16) becomes

$$\begin{aligned} s \|d_t \mathbf{A}_h^{n+1}\|^2 &+ \frac{s\eta}{2\delta t} (\|\nabla \times \mathbf{A}_h^{n+1}\|^2 + \|\nabla \times (\mathbf{A}_h^{n+1} - \mathbf{A}_h^n)\|^2 - \|\nabla \times \mathbf{A}_h^n\|^2) \\ &+ s^2 \delta t \|\nabla \times \mathbf{A}_h^n \times d_t \mathbf{A}_h^{n+1}\|^2 + \frac{1}{2\delta t} (\|\mathbf{u}_h^{n+1}\|^2 + \|\tilde{\mathbf{u}}_h^{n+1} - \mathbf{u}_h^n\|^2 - \|\mathbf{u}_h^n\|^2) + \nu \|\nabla \tilde{\mathbf{u}}_h^{n+1}\|^2 \\ &+ \frac{\delta t}{2} \|\nabla p_h^{n+1}\|^2 - \frac{\delta t}{2} \|\nabla p_h^n\|^2 + s \|\nabla \times \mathbf{A}_h^n \times \tilde{\mathbf{u}}_h^{n+1}\|^2 \\ &+ s(\nabla \times \mathbf{A}_h^n \times (\mathbf{u}_h^n - \tilde{\mathbf{u}}_h^{n+1}), d_t \mathbf{A}_h^{n+1}) + 2s(\nabla \times \mathbf{A}_h^n \times \tilde{\mathbf{u}}_h^{n+1}, d_t \mathbf{A}_h^{n+1}) = 0. \end{aligned} \tag{3.17}$$

Note  $s \|d_t \mathbf{A}_h^{n+1}\|^2 + 2s(\nabla \times \mathbf{A}_h^n \times \tilde{\mathbf{u}}_h^{n+1}, d_t \mathbf{A}_h^{n+1}) + s \|\nabla \times \mathbf{A}_h^n \times \tilde{\mathbf{u}}_h^{n+1}\|^2 = s \|d_t \mathbf{A}_h^{n+1} + \nabla \times \mathbf{A}_h^n \times \tilde{\mathbf{u}}_h^{n+1}\|^2$ , (3.17) becomes

$$\begin{aligned} &\frac{s\eta}{2\delta t} (\|\nabla \times \mathbf{A}_h^{n+1}\|^2 + \|\nabla \times (\mathbf{A}_h^{n+1} - \mathbf{A}_h^n)\|^2 - \|\nabla \times \mathbf{A}_h^n\|^2) + s^2 \delta t \|\nabla \times \mathbf{A}_h^n \times d_t \mathbf{A}_h^{n+1}\|^2 \\ &+ \frac{1}{2\delta t} (\|\mathbf{u}_h^{n+1}\|^2 + \|\tilde{\mathbf{u}}_h^{n+1} - \mathbf{u}_h^n\|^2 - \|\mathbf{u}_h^n\|^2) + \nu \|\nabla \tilde{\mathbf{u}}_h^{n+1}\|^2 \\ &+ \frac{\delta t}{2} \|\nabla p_h^{n+1}\|^2 - \frac{\delta t}{2} \|\nabla p_h^n\|^2 + s \|d_t \mathbf{A}_h^{n+1} + \nabla \times \mathbf{A}_h^n \times \tilde{\mathbf{u}}_h^{n+1}\|^2 \\ &= s(\nabla \times \mathbf{A}_h^n \times (\tilde{\mathbf{u}}_h^{n+1} - \mathbf{u}_h^n), d_t \mathbf{A}_h^{n+1}). \end{aligned} \tag{3.18}$$

The last term in (3.18) is estimated as

$$\begin{aligned} s(\nabla \times \mathbf{A}_h^n \times (\tilde{\mathbf{u}}_h^{n+1} - \mathbf{u}_h^n), d_t \mathbf{A}_h^{n+1}) &\leq s \|\nabla \times \mathbf{A}_h^n \times d_t \mathbf{A}_h^{n+1}\| \|\tilde{\mathbf{u}}_h^{n+1} - \mathbf{u}_h^n\| \\ &\leq \frac{1}{2\delta t} \|\tilde{\mathbf{u}}_h^{n+1} - \mathbf{u}_h^n\|^2 + \frac{\delta t}{2} s^2 \|\nabla \times \mathbf{A}_h^n \times d_t \mathbf{A}_h^{n+1}\|^2. \end{aligned} \tag{3.19}$$

By combining (3.18) with (3.19), we obtain

$$\begin{aligned} &\frac{s\eta}{2\delta t} (\|\nabla \times \mathbf{A}_h^{n+1}\|^2 + \|\nabla \times (\mathbf{A}_h^{n+1} - \mathbf{A}_h^n)\|^2 - \|\nabla \times \mathbf{A}_h^n\|^2) + \frac{\delta t}{2} s^2 \|\nabla \times \mathbf{A}_h^n \times d_t \mathbf{A}_h^{n+1}\|^2 \\ &+ \frac{1}{2\delta t} (\|\mathbf{u}_h^{n+1}\|^2 - \|\mathbf{u}_h^n\|^2) + \nu \|\nabla \tilde{\mathbf{u}}_h^{n+1}\|^2 + \frac{\delta t}{2} \|\nabla p_h^{n+1}\|^2 - \frac{\delta t}{2} \|\nabla p_h^n\|^2 \\ &+ s \|d_t \mathbf{A}_h^{n+1} + \nabla \times \mathbf{A}_h^n \times \tilde{\mathbf{u}}_h^{n+1}\|^2 \leq 0. \end{aligned} \tag{3.20}$$

After dropping some positive terms in (3.20), we arrive at

$$\begin{aligned} &s\eta \|\nabla \times \mathbf{A}_h^{n+1}\|^2 + \|\mathbf{u}_h^{n+1}\|^2 + \delta t^2 \|\nabla p_h^{n+1}\|^2 + 2\delta t \nu \|\nabla \tilde{\mathbf{u}}_h^{n+1}\|^2 \\ &+ 2\delta t s \|d_t \mathbf{A}_h^{n+1} + \nabla \times \mathbf{A}_h^n \times \tilde{\mathbf{u}}_h^{n+1}\|^2 \\ &\leq s\eta \|\nabla \times \mathbf{A}_h^n\|^2 + \|\mathbf{u}_h^n\|^2 + \delta t^2 \|\nabla p_h^n\|^2. \end{aligned}$$

The proof is completed. □

**Remark 3.6.** In the proof of above theorem, we observe that the introduced first order implicit-explicit stabilized term  $s\nabla \times \mathbf{A}_h^n \times ((\mathbf{A}_h^{n+1} - \mathbf{A}_h^n) \times \nabla \times \mathbf{A}_h^n)$  generates a positive term  $\delta t s^2 \|\nabla \times \mathbf{A}_h^n \times d_t \mathbf{A}_h^{n+1}\|^2$ . From (3.19), this positive term plays an important role in controlling the last term of (3.18). Thus, we obtain the unconditional energy stability of the scheme (3.6)-(3.9).

## 3.2 Second-order fully-discrete schemes

In this section, we further propose two second-order, linear, unconditionally energy stable, but “partially” decoupled schemes for the model (2.1)-(2.5). For convenience, we omit the subscript  $_h$  for all variables.

### 3.2.1 Crank-Nicolson scheme

The first second-order fully-discrete scheme is developed based on the Crank-Nicolson formulation for the time derivative that reads as follows.

We denote  $\hat{w}^n = \frac{3}{2}w^n - \frac{1}{2}w^{n-1}$  and get  $(\mathbf{u}^1, p^1, \mathbf{A}^1) \in \mathbf{V}_h \times Q_h \times \mathbf{C}_h$  by any first-order scheme.

*Step 1.* Solve  $(\tilde{\mathbf{u}}^{n+1}, \mathbf{A}^{n+1}) \in \mathbf{V}_h \times \mathbf{C}_h$  such that for  $\forall (\mathbf{v}, \boldsymbol{\phi}) \in \mathbf{V}_h \times \mathbf{C}_h$

$$\begin{aligned} \left( \frac{\tilde{\mathbf{u}}^{n+1} - \mathbf{u}^n}{\delta t}, \mathbf{v} \right) + \nu \left( \nabla \frac{\tilde{\mathbf{u}}^{n+1} + \mathbf{u}^n}{2}, \nabla \mathbf{v} \right) + b \left( \hat{\mathbf{u}}^n, \frac{\tilde{\mathbf{u}}^{n+1} + \mathbf{u}^n}{2}, \mathbf{v} \right) + (\nabla p^n, \mathbf{v}) \\ + s \left( d_t \mathbf{A}^{n+1} + \nabla \times \hat{\mathbf{A}}^n \times \frac{\tilde{\mathbf{u}}^{n+1} + \mathbf{u}^n}{2}, \nabla \times \hat{\mathbf{A}}^n \times \mathbf{v} \right) = 0, \quad (3.21) \\ (d_t \mathbf{A}^{n+1}, \boldsymbol{\phi}) + \eta \left( \nabla \times \frac{\mathbf{A}^{n+1} + \mathbf{A}^n}{2}, \nabla \times \boldsymbol{\phi} \right) + \left( \nabla \times \hat{\mathbf{A}}^n \times \frac{\tilde{\mathbf{u}}^{n+1} + \mathbf{u}^n}{2}, \boldsymbol{\phi} \right) = 0. \end{aligned}$$

*Step 2.* Find  $(\mathbf{u}^{n+1}, p^{n+1}) \in \mathbf{V}_h \times Q_h$  such that for  $\forall (\mathbf{v}, q) \in \mathbf{V}_h \times Q_h$

$$\begin{aligned} \left( \frac{\mathbf{u}^{n+1} - \tilde{\mathbf{u}}^{n+1}}{\delta t}, \mathbf{v} \right) + \frac{1}{2} (\nabla p^{n+1} - \nabla p^n, \mathbf{v}) = 0, \quad (3.22) \\ (\nabla \cdot \mathbf{u}^{n+1}, q) = 0. \end{aligned}$$

The scheme (3.21)-(3.22) is linear and second-order, but partially decoupled. It is still unconditionally energy stable and the stability result is shown as follows. To prove the stability, we define the  $L^2$  orthogonal projection operator  $P :: L^2(\Omega)^3 \rightarrow \mathbf{V}_h : \forall \mathbf{f} \in L^2(\Omega)^3$ , find  $P\mathbf{f} \in \mathbf{V}_h$  such that

$$(P\mathbf{f}, \mathbf{v}) = (\mathbf{f}, \mathbf{v}), \quad \forall \mathbf{v} \in \mathbf{V}_h.$$

**Theorem 3.3.** *The scheme (3.21)-(3.22) is unconditionally energy stable in the sense that*

$$\begin{aligned} & E(\mathbf{u}^{n+1}, \mathbf{A}^{n+1}) + \frac{\delta t^2}{8} \|P(\nabla p^{n+1})\|^2 + \delta t \nu \left\| \nabla \frac{\tilde{\mathbf{u}}^{n+1} + \mathbf{u}^n}{2} \right\|^2 \\ & + \delta t s \left\| d_t \mathbf{A}^{n+1} + \nabla \times \hat{\mathbf{A}}^n \times \frac{\tilde{\mathbf{u}}^{n+1} + \mathbf{u}^n}{2} \right\|^2 \\ & = E(\mathbf{u}^n, \mathbf{A}^n) + \frac{\delta t^2}{8} \|P(\nabla p^n)\|^2. \end{aligned} \tag{3.23}$$

*Proof.* Taking  $\mathbf{v} = \frac{\tilde{\mathbf{u}}^{n+1} + \mathbf{u}^n}{2}$ ,  $\boldsymbol{\phi} = s d_t \mathbf{A}^{n+1}$  in (3.21), and using the second equation in (3.22), we get

$$\begin{aligned} & \frac{1}{2\delta t} (\|\tilde{\mathbf{u}}^{n+1}\|^2 - \|\mathbf{u}^n\|^2) + \nu \left\| \nabla \frac{\tilde{\mathbf{u}}^{n+1} + \mathbf{u}^n}{2} \right\|^2 + \frac{1}{2} (\nabla p^n, \tilde{\mathbf{u}}^{n+1}) \\ & + s \left( d_t \mathbf{A}^{n+1} + \nabla \times \hat{\mathbf{A}}^n \times \frac{\tilde{\mathbf{u}}^{n+1} + \mathbf{u}^n}{2}, \nabla \times \hat{\mathbf{A}}^n \times \frac{\tilde{\mathbf{u}}^{n+1} + \mathbf{u}^n}{2} \right) = 0, \end{aligned} \tag{3.24}$$

and

$$\frac{s\eta}{2\delta t} (\|\nabla \times \mathbf{A}^{n+1}\|^2 - \|\nabla \times \mathbf{A}^n\|^2) + s \left( d_t \mathbf{A}^{n+1} + \nabla \times \hat{\mathbf{A}}^n \times \frac{\tilde{\mathbf{u}}^{n+1} + \mathbf{u}^n}{2}, d_t \mathbf{A}^{n+1} \right) = 0. \tag{3.25}$$

The first equation in (3.22) implies

$$P \left( \frac{\mathbf{u}^{n+1} - \tilde{\mathbf{u}}^{n+1}}{\delta t} + \frac{1}{2} \nabla p^{n+1} - \frac{1}{2} \nabla p^n \right) = 0,$$

which can be written as

$$\mathbf{u}^{n+1} + \frac{\delta t}{2} P(\nabla p^{n+1}) = \tilde{\mathbf{u}}^{n+1} + \frac{\delta t}{2} P(\nabla p^n). \tag{3.26}$$

By taking the  $L^2$  inner product of (3.26) with itself on both sides, and using  $(\mathbf{u}^{n+1}, P(\nabla p^{n+1})) = (\mathbf{u}^{n+1}, \nabla p^{n+1}) = -(\nabla \cdot \mathbf{u}^{n+1}, p^{n+1}) = 0$ ,  $(\tilde{\mathbf{u}}^{n+1}, P(\nabla p^n)) = (\tilde{\mathbf{u}}^{n+1}, \nabla p^n)$ , we get

$$\frac{1}{2} (\tilde{\mathbf{u}}^{n+1}, \nabla p^n) = \frac{1}{2\delta t} \|\mathbf{u}^{n+1}\|^2 - \frac{1}{2\delta t} \|\tilde{\mathbf{u}}^{n+1}\|^2 + \frac{\delta t}{8} \|P(\nabla p^{n+1})\|^2 - \frac{\delta t}{8} \|P(\nabla p^n)\|^2. \tag{3.27}$$

By taking the summations of (3.24), (3.25) and (3.27), we derive

$$\begin{aligned} & \frac{1}{2\delta t} (\|\mathbf{u}^{n+1}\|^2 - \|\mathbf{u}^n\|^2) + \frac{s\eta}{2\delta t} (\|\nabla \times \mathbf{A}^{n+1}\|^2 - \|\nabla \times \mathbf{A}^n\|^2) + \nu \left\| \nabla \frac{\tilde{\mathbf{u}}^{n+1} + \mathbf{u}^n}{2} \right\|^2 \\ & + s \left\| d_t \mathbf{A}^{n+1} + \nabla \times \hat{\mathbf{A}}^n \times \frac{\tilde{\mathbf{u}}^{n+1} + \mathbf{u}^n}{2} \right\|^2 + \frac{\delta t}{8} \|P(\nabla p^{n+1})\|^2 - \frac{\delta t}{8} \|P(\nabla p^n)\|^2 = 0. \end{aligned} \tag{3.28}$$

We complete the proof by multiplying  $\delta t$ . □

For (3.21) in *Step 1*, we shall solve the following coupled problem at each time step: find  $(\mathbf{u}, \mathbf{A}) \in \mathbf{V}_h \times \mathbf{C}_h$  such that for  $\forall (\mathbf{v}, \boldsymbol{\phi}) \in \mathbf{V}_h \times \mathbf{C}_h$ ,

$$\begin{cases} \frac{1}{\delta t}(\mathbf{u}, \mathbf{v}) + \frac{\nu}{2}(\nabla \mathbf{u}, \nabla \mathbf{v}) + \frac{1}{2}b(\widehat{\mathbf{u}}^n, \mathbf{u}, \mathbf{v}) + \frac{s}{\delta t}(\mathbf{A}, \nabla \times \widehat{\mathbf{A}}^n \times \mathbf{v}) \\ \quad + \frac{s}{2}(\nabla \times \widehat{\mathbf{A}}^n \times \mathbf{u}, \nabla \times \widehat{\mathbf{A}}^n \times \mathbf{v}) = (L_1^n, \mathbf{v}), \\ \frac{1}{\delta t}(\mathbf{A}, \boldsymbol{\phi}) + \frac{\eta}{2}(\nabla \times \mathbf{A}, \nabla \times \boldsymbol{\phi}) + \frac{1}{2}(\nabla \times \widehat{\mathbf{A}}^n \times \mathbf{u}, \boldsymbol{\phi}) = (L_2^n, \boldsymbol{\phi}), \end{cases} \quad (3.29)$$

where

$$\begin{aligned} (L_1^n, \mathbf{v}) &= \frac{1}{\delta t}(\mathbf{u}^n, \mathbf{v}) - \frac{\nu}{2}(\nabla \mathbf{u}^n, \nabla \mathbf{v}) - \frac{1}{2}b(\widehat{\mathbf{u}}^n, \mathbf{u}^n, \mathbf{v}) - (\nabla p^n, \mathbf{v}) + \frac{s}{\delta t}(\mathbf{A}^n, \nabla \times \widehat{\mathbf{A}}^n \times \mathbf{v}) \\ &\quad - \frac{s}{2}(\nabla \times \widehat{\mathbf{A}}^n \times \mathbf{u}^n, \nabla \times \widehat{\mathbf{A}}^n \times \mathbf{v}), \\ (L_2^n, \boldsymbol{\phi}) &= \frac{1}{\delta t}(\mathbf{A}^n, \boldsymbol{\phi}) - \frac{\eta}{2}(\nabla \times \mathbf{A}^n, \nabla \times \boldsymbol{\phi}) - \frac{1}{2}(\nabla \times \widehat{\mathbf{A}}^n \times \mathbf{u}^n, \boldsymbol{\phi}). \end{aligned}$$

To avoid solving this coupled problem, we present the following decoupled iteration algorithm.

*Step I.* Set  $\mathbf{u}_0 = \mathbf{u}^n$ ,  $\mathbf{A}_0 = \mathbf{A}^n$  and a given tolerance constant  $\epsilon \ll 1$ .

*Step II.* Having computed  $\mathbf{u}_{k-1}, \mathbf{A}_{k-1}$ , we compute  $\mathbf{u}_k \in \mathbf{V}_h$  and  $\mathbf{A}_k \in \mathbf{C}_h$  from

$$\begin{aligned} \frac{1}{\delta t}(\mathbf{u}_k, \mathbf{v}) + \frac{\nu}{2}(\nabla \mathbf{u}_k, \nabla \mathbf{v}) + \frac{1}{2}b(\widehat{\mathbf{u}}^n, \mathbf{u}_k, \mathbf{v}) + \frac{s}{\delta t}(\mathbf{A}_{k-1}, \nabla \times \widehat{\mathbf{A}}^n \times \mathbf{v}) \\ + \frac{s}{2}(\nabla \times \widehat{\mathbf{A}}^n \times \mathbf{u}_k, \nabla \times \widehat{\mathbf{A}}^n \times \mathbf{v}) = (L_1^n, \mathbf{v}), \end{aligned} \quad (3.30)$$

$$\frac{1}{\delta t}(\mathbf{A}_k, \boldsymbol{\phi}) + \frac{\eta}{2}(\nabla \times \mathbf{A}_k, \nabla \times \boldsymbol{\phi}) + \frac{1}{2}(\nabla \times \widehat{\mathbf{A}}^n \times \mathbf{u}_{k-1}, \boldsymbol{\phi}) = (L_2^n, \boldsymbol{\phi}). \quad (3.31)$$

*Step III.* If  $\|\mathbf{u}_k - \mathbf{u}_{k-1}\| + \|\mathbf{A}_k - \mathbf{A}_{k-1}\| \leq \epsilon$ , stop and set  $\tilde{\mathbf{u}}^{n+1} = \mathbf{u}_k, \mathbf{A}^{n+1} = \mathbf{A}_k$ , else set  $\mathbf{u}_{k-1} = \mathbf{u}_k, \mathbf{A}_{k-1} = \mathbf{A}_k, k = k + 1$  and go to *Step II*.

### 3.2.2 BDF2 scheme

We further develop another second-order version scheme based on the Adam-Bashforth (BDF2) formulations, that reads as follows.

We denote  $w_{2,1}^n = 2w^n - w^{n-1}$  and compute  $(\mathbf{u}^1, p^1, \mathbf{A}^1) \in \mathbf{V}_h \times Q_h \times \mathbf{C}_h$  by any first-order scheme.

Step 1. Solve  $(\tilde{\mathbf{u}}^{n+1}, \mathbf{A}^{n+1}) \in \mathbf{V}_h \times \mathbf{C}_h$  such that for  $\forall (\mathbf{v}, \boldsymbol{\phi}) \in \mathbf{V}_h \times \mathbf{C}_h$

$$\left( \frac{3\tilde{\mathbf{u}}^{n+1} - 4\mathbf{u}^n + \mathbf{u}^{n-1}}{2\delta t}, \mathbf{v} \right) + \nu(\nabla \tilde{\mathbf{u}}^{n+1}, \nabla \mathbf{v}) + b(\mathbf{u}_{2,1}^n, \tilde{\mathbf{u}}^{n+1}, \mathbf{v}) + (\nabla p^n, \mathbf{v}) + s \left( \frac{3\mathbf{A}^{n+1} - 4\mathbf{A}^n + \mathbf{A}^{n-1}}{2\delta t} \times \nabla \times \mathbf{A}_{2,1}^n, \mathbf{v} \right) + s(\nabla \times \mathbf{A}_{2,1}^n \times \tilde{\mathbf{u}}^{n+1}, \nabla \times \mathbf{A}_{2,1}^n \times \mathbf{v}) = 0, \quad (3.32)$$

$$\left( \frac{3\mathbf{A}^{n+1} - 4\mathbf{A}^n + \mathbf{A}^{n-1}}{2\delta t}, \boldsymbol{\phi} \right) + \eta(\nabla \times \mathbf{A}^{n+1}, \nabla \times \boldsymbol{\phi}) + (\nabla \times \mathbf{A}_{2,1}^n \times \tilde{\mathbf{u}}^{n+1}, \boldsymbol{\phi}) = 0. \quad (3.33)$$

Step 2. Find  $p^{n+1} \in Q_h$  such that for  $\forall q \in Q_h$

$$(\nabla p^{n+1}, \nabla q) = -\frac{3}{2\delta t}(\nabla \cdot \tilde{\mathbf{u}}^{n+1}, q) + (\nabla p^n, \nabla q). \quad (3.34)$$

Step 3. Update  $\mathbf{u}^{n+1} \in \mathbf{V}_h + \nabla Q_h$  from

$$\mathbf{u}^{n+1} = \tilde{\mathbf{u}}^{n+1} - \frac{2}{3}\delta t \nabla p^{n+1} + \frac{2}{3}\delta t \nabla p^n. \quad (3.35)$$

**Remark 3.7.** Similar to the first order scheme, the final velocity field  $\mathbf{u}^{n+1}$  in the BDF2 scheme also satisfies the discrete divergence free condition as well. This can be deduced by taking the  $L^2$  inner product of (3.35) with  $\nabla q, \forall q \in Q_h$ , we obtain

$$(\mathbf{u}^{n+1}, \nabla q) = -(\nabla \cdot \tilde{\mathbf{u}}^{n+1}, q) - \frac{2}{3}\delta t(\nabla(p^{n+1} - p^n), \nabla q).$$

In view of (3.34), we arrive at

$$(\mathbf{u}^{n+1}, \nabla q) = 0, \quad \forall q \in Q_h. \quad (3.36)$$

The unconditional energy stability of the scheme (3.32)-(3.35) is stated as follows.

**Theorem 3.4.** *The scheme (3.32)-(3.35) is unconditionally energy stable in the sense that*

$$\begin{aligned} & \|\mathbf{u}^{n+1}\|^2 + s\eta\|\nabla \times \mathbf{A}^{n+1}\|^2 + \|\mathbf{u}_{2,1}^{n+1}\|^2 + s\eta\|\nabla \times \mathbf{A}_{2,1}^{n+1}\|^2 + \frac{4\delta t^2}{3}\|\nabla p^{n+1}\|^2 \\ & + 4\delta t\nu\|\nabla \tilde{\mathbf{u}}^{n+1}\|^2 + 4\delta ts\left\| \frac{3\mathbf{A}^{n+1} - 4\mathbf{A}^n + \mathbf{A}^{n-1}}{2\delta t} + \nabla \times \mathbf{A}_{2,1}^n \times \tilde{\mathbf{u}}^{n+1} \right\|^2 \\ & \leq \|\mathbf{u}^n\|^2 + s\eta\|\nabla \times \mathbf{A}^n\|^2 + \|\mathbf{u}_{2,1}^n\|^2 + s\eta\|\nabla \times \mathbf{A}_{2,1}^n\|^2 + \frac{4\delta t^2}{3}\|\nabla p^n\|^2. \end{aligned}$$

*Proof.* Taking  $\mathbf{v} = \tilde{\mathbf{u}}^{n+1}$  in (3.32) and  $\boldsymbol{\phi} = s\frac{3\mathbf{A}^{n+1} - 4\mathbf{A}^n + \mathbf{A}^{n-1}}{2\delta t}$  in (3.33), and using the identity

$$\begin{aligned} & (3w^{n+1} - 4w^n + w^{n-1}, 2w^{n+1}) \\ & = \|w^{n+1}\|^2 - \|w^n\|^2 + \|w_{2,1}^{n+1}\|^2 - \|w_{2,1}^n\|^2 + \|w^{n+1} - 2w^n + w^{n-1}\|^2, \end{aligned}$$

we obtain

$$\left( \frac{3\tilde{\mathbf{u}}^{n+1} - 4\mathbf{u}^n + \mathbf{u}^{n-1}}{2\delta t}, \tilde{\mathbf{u}}^{n+1} \right) + \nu \|\nabla \tilde{\mathbf{u}}^{n+1}\|^2 + s \left( \nabla \times \mathbf{A}_{2,1}^n \times \tilde{\mathbf{u}}^{n+1}, \frac{3\mathbf{A}^{n+1} - 4\mathbf{A}^n + \mathbf{A}^{n-1}}{2\delta t} \right) \\ + (\nabla p^n, \tilde{\mathbf{u}}^{n+1}) + s (\nabla \times \mathbf{A}_{2,1}^n \times \tilde{\mathbf{u}}^{n+1}, \nabla \times \mathbf{A}_{2,1}^n \times \tilde{\mathbf{u}}^{n+1}) = 0,$$

and

$$\frac{s\eta}{4\delta t} (\|\nabla \times \mathbf{A}^{n+1}\|^2 - \|\nabla \times \mathbf{A}^n\|^2 + \|\nabla \times \mathbf{A}_{2,1}^{n+1}\|^2 - \|\nabla \times \mathbf{A}_{2,1}^n\|^2 + \|\nabla \times (\mathbf{A}^{n+1} - 2\mathbf{A}^n + \mathbf{A}^{n-1})\|^2) \\ + s \left( \frac{3\mathbf{A}^{n+1} - 4\mathbf{A}^n + \mathbf{A}^{n-1}}{2\delta t} + \nabla \times \mathbf{A}_{2,1}^n \times \tilde{\mathbf{u}}^{n+1}, \frac{3\mathbf{A}^{n+1} - 4\mathbf{A}^n + \mathbf{A}^{n-1}}{2\delta t} \right) = 0.$$

By taking the summation of the above two equations, we obtain

$$\left( \frac{3\tilde{\mathbf{u}}^{n+1} - 4\mathbf{u}^n + \mathbf{u}^{n-1}}{2\delta t}, \tilde{\mathbf{u}}^{n+1} \right) + \nu \|\nabla \tilde{\mathbf{u}}^{n+1}\|^2 + (\nabla p^n, \tilde{\mathbf{u}}^{n+1}) \\ + \frac{s\eta}{4\delta t} (\|\nabla \times \mathbf{A}^{n+1}\|^2 - \|\nabla \times \mathbf{A}^n\|^2 + \|\nabla \times \mathbf{A}_{2,1}^{n+1}\|^2 - \|\nabla \times \mathbf{A}_{2,1}^n\|^2) \\ + \frac{s\eta}{4\delta t} \|\nabla \times (\mathbf{A}^{n+1} - 2\mathbf{A}^n + \mathbf{A}^{n-1})\|^2 \\ + s \left\| \frac{3\mathbf{A}^{n+1} - 4\mathbf{A}^n + \mathbf{A}^{n-1}}{2\delta t} + \nabla \times \mathbf{A}_{2,1}^n \times \tilde{\mathbf{u}}^{n+1} \right\|^2 = 0. \quad (3.37)$$

By rewriting (3.35) as  $\tilde{\mathbf{u}}^{n+1} - \mathbf{u}^{n+1} = \frac{2}{3}\delta t \nabla(p^{n+1} - p^n)$  and taking the  $L^2$  inner product of it with  $\mathbf{u}^{n+1}$ , we derive

$$(\tilde{\mathbf{u}}^{n+1} - \mathbf{u}^{n+1}, \mathbf{u}^{n+1}) = \frac{2}{3}\delta t (\nabla(p^{n+1} - p^n), \mathbf{u}^{n+1}) = 0, \quad (3.38)$$

and

$$0 = (3\mathbf{u}^{n+1} - 4\mathbf{u}^n + \mathbf{u}^{n-1}, \tilde{\mathbf{u}}^{n+1} - \mathbf{u}^{n+1}) \\ = (3\mathbf{u}^{n+1} - 4\mathbf{u}^n + \mathbf{u}^{n-1}, \frac{2}{3}\delta t \nabla(p^{n+1} - p^n)) \\ = 2\delta t (\mathbf{u}^{n+1}, \nabla(p^{n+1} - p^n)) - \frac{8}{3}\delta t (\mathbf{u}^n, \nabla(p^{n+1} - p^n)) + \frac{2}{3}\delta t (\mathbf{u}^{n-1}, \nabla(p^{n+1} - p^n)), \quad (3.39)$$

where (3.36) is used.

Using (3.38) and (3.39), we deduce

$$\begin{aligned}
 & (3\tilde{\mathbf{u}}^{n+1} - 4\mathbf{u}^n + \mathbf{u}^{n-1}, \tilde{\mathbf{u}}^{n+1}) \\
 &= (3\tilde{\mathbf{u}}^{n+1} - 3\mathbf{u}^{n+1}, \tilde{\mathbf{u}}^{n+1}) + (3\mathbf{u}^{n+1} - 4\mathbf{u}^n + \mathbf{u}^{n-1}, \tilde{\mathbf{u}}^{n+1}) \\
 &= (3\tilde{\mathbf{u}}^{n+1} - 3\mathbf{u}^{n+1}, \tilde{\mathbf{u}}^{n+1} + \mathbf{u}^{n+1}) + (3\mathbf{u}^{n+1} - 4\mathbf{u}^n + \mathbf{u}^{n-1}, \mathbf{u}^{n+1}) \\
 &= \frac{1}{2} (\|\mathbf{u}^{n+1}\|^2 - \|\mathbf{u}^n\|^2 + \|\mathbf{u}_{2,1}^{n+1}\|^2 - \|\mathbf{u}_{2,1}^n\|^2 + \|\mathbf{u}^{n+1} - 2\mathbf{u}^n + \mathbf{u}^{n-1}\|^2) \\
 &\quad + 3\|\tilde{\mathbf{u}}^{n+1}\|^2 - 3\|\mathbf{u}^{n+1}\|^2.
 \end{aligned} \tag{3.40}$$

We rewrite (3.35) as

$$\mathbf{u}^{n+1} + \frac{2}{3}\delta t \nabla p^{n+1} = \tilde{\mathbf{u}}^{n+1} + \frac{2}{3}\delta t \nabla p^n.$$

Taking the  $L^2$  inner product of the above equation with itself, we derive

$$(\tilde{\mathbf{u}}^{n+1}, \nabla p^n) = \frac{3}{4\delta t} \|\mathbf{u}^{n+1}\|^2 - \frac{3}{4\delta t} \|\tilde{\mathbf{u}}^{n+1}\|^2 + \frac{\delta t}{3} \|\nabla p^{n+1}\|^2 - \frac{\delta t}{3} \|\nabla p^n\|^2. \tag{3.41}$$

Combining (3.37), (3.40) with (3.41), we obtain

$$\begin{aligned}
 & \frac{1}{4\delta t} (\|\mathbf{u}^{n+1}\|^2 - \|\mathbf{u}^n\|^2 + \|\mathbf{u}_{2,1}^{n+1}\|^2 - \|\mathbf{u}_{2,1}^n\|^2 + \|\mathbf{u}^{n+1} - 2\mathbf{u}^n + \mathbf{u}^{n-1}\|^2) \\
 &+ \frac{3}{4\delta t} \|\tilde{\mathbf{u}}^{n+1}\|^2 - \frac{3}{4\delta t} \|\mathbf{u}^{n+1}\|^2 + \nu \|\nabla \tilde{\mathbf{u}}^{n+1}\|^2 + \frac{\delta t}{3} \|\nabla p^{n+1}\|^2 - \frac{\delta t}{3} \|\nabla p^n\|^2 \\
 &+ \frac{s\eta}{4\delta t} (\|\nabla \times \mathbf{A}^{n+1}\|^2 - \|\nabla \times \mathbf{A}^n\|^2 + \|\nabla \times \mathbf{A}_{2,1}^{n+1}\|^2 - \|\nabla \times \mathbf{A}_{2,1}^n\|^2) \\
 &+ \frac{s\eta}{4\delta t} \|\nabla \times (\mathbf{A}^{n+1} - 2\mathbf{A}^n + \mathbf{A}^{n-1})\|^2 + s \left\| \frac{3\mathbf{A}^{n+1} - 4\mathbf{A}^n + \mathbf{A}^{n-1}}{2\delta t} + \nabla \times \mathbf{A}_{2,1}^n \times \tilde{\mathbf{u}}^{n+1} \right\|^2 = 0.
 \end{aligned} \tag{3.42}$$

We also rewrite (3.35) as

$$\mathbf{u}^{n+1} - \tilde{\mathbf{u}}^{n+1} = -\frac{2}{3}\delta t \nabla p^{n+1} + \frac{2}{3}\delta t \nabla p^n.$$

By taking the  $L^2$  inner product of the above equation with  $\mathbf{u}^{n+1}$ , and in view of (3.36), we obtain

$$\|\mathbf{u}^{n+1} - \tilde{\mathbf{u}}^{n+1}\|^2 + \|\mathbf{u}^{n+1}\|^2 - \|\tilde{\mathbf{u}}^{n+1}\|^2 = 0. \tag{3.43}$$

Finally, by combining (3.42) and (3.43), we obtain

$$\begin{aligned} & \frac{1}{4\delta t} (\|\mathbf{u}^{n+1}\|^2 - \|\mathbf{u}^n\|^2 + \|\mathbf{u}_{2,1}^{n+1}\|^2 - \|\mathbf{u}_{2,1}^n\|^2 + \|\mathbf{u}^{n+1} - 2\mathbf{u}^n + \mathbf{u}^{n-1}\|^2) \\ & \frac{3}{4\delta t} \|\tilde{\mathbf{u}}^{n+1} - \mathbf{u}^{n+1}\|^2 + \nu \|\nabla \tilde{\mathbf{u}}^{n+1}\|^2 + \frac{\delta t}{3} \|\nabla p^{n+1}\|^2 - \frac{\delta t}{3} \|\nabla p^n\|^2 \\ & \frac{s\eta}{4\delta t} (\|\nabla \times \mathbf{A}^{n+1}\|^2 - \|\nabla \times \mathbf{A}^n\|^2 + \|\nabla \times \mathbf{A}_{2,1}^{n+1}\|^2 - \|\nabla \times \mathbf{A}_{2,1}^n\|^2) \\ & \frac{s\eta}{4\delta t} \|\nabla \times (\mathbf{A}^{n+1} - 2\mathbf{A}^n + \mathbf{A}^{n-1})\|^2 + s \left\| \frac{3\mathbf{A}^{n+1} - 4\mathbf{A}^n + \mathbf{A}^{n-1}}{2\delta t} + \nabla \times \mathbf{A}_{2,1}^n \times \tilde{\mathbf{u}}^{n+1} \right\|^2 = 0. \end{aligned}$$

After dropping several positive terms, we arrive at the energy stability.  $\square$

The implementation of (3.32)-(3.33) in *Step 1* is similar to the Crank-Nicolson scheme, we omit the details here.

## 4 Numerical simulations

In this section, we present a series of 3D numerical simulations to show the stability and accuracy of the developed schemes. We use Taylor-Hood element [10] for  $V_h$  and  $Q_h$  that satisfies *inf-sup* condition (3.5), and use the first-order  $H(\text{curl})$ -conforming Nédélec edge element [25, 27] for  $C_h$ . With these finite element spaces, the optimal convergence rates for the developed first-order and second-order schemes are expected to be

$$\text{First-order scheme: } \begin{cases} \|e_u\|_{L^2} \sim h^3 + \delta t, & \|e_u\|_{H^1} \sim h^2 + \delta t, & \|e_p\|_{L^2} \sim h^2 + \delta t, \\ \|e_A\|_{L^2} \sim h + \delta t, & \|e_A\|_{\text{curl}} \sim h + \delta t. \end{cases} \quad (4.1)$$

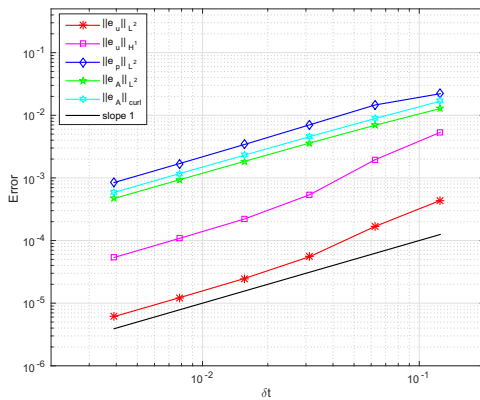
$$\text{Second-order scheme: } \begin{cases} \|e_u\|_{L^2} \sim h^3 + \delta t^2, & \|e_u\|_{H^1} \sim h^2 + \delta t^2, & \|e_p\|_{L^2} \sim h^2 + \delta t^2, \\ \|e_A\|_{L^2} \sim h + \delta t^2, & \|e_A\|_{\text{curl}} \sim h + \delta t^2. \end{cases} \quad (4.2)$$

Here  $e_\psi = \psi(t_n) - \psi_h^n$  for any vector or scalar function  $\psi$  at  $t = t^n$ .

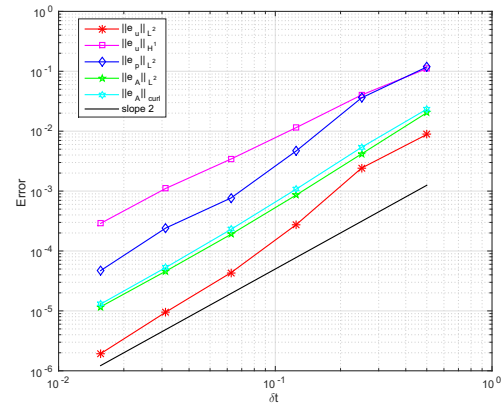
In Sections 4.1 and 4.2, we verify the temporal and spatial convergence orders for the proposed schemes, respectively. In Section 4.3, we perform stability tests to show the unconditional energy stability of the schemes. Finally, in Sections 4.4-4.5, two benchmark problems, driven cavity flow and Kelvin-Helmholtz instability, are simulated by the first-order scheme (3.6)-(3.9). All numerical simulations are implemented by FEniCS Project [23].

### 4.1 Temporal accuracy tests

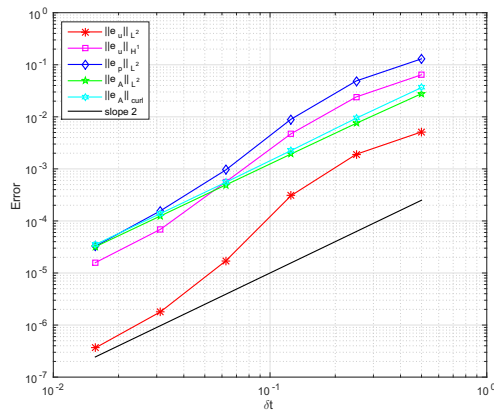
We first verify the temporal convergence orders. The 3D computational domain  $\Omega$  is set as  $[0,1]^3$ , and the parameters are set as  $R_e = R_m = s = 1$ . The source terms and boundary



(a) First-order scheme.



(b) Crank-Nicolson scheme.



(c) BDF2 scheme.

Figure 1: The numerical errors of  $\|e_u\|_{L^2}$ ,  $\|e_u\|_{H^1}$ ,  $\|e_p\|_{L^2}$ ,  $\|e_A\|_{L^2}$  and  $\|e_A\|_{curl}$  at  $t=1$  that are computed by using various temporal resolutions with the given exact solutions of (4.3).

conditions are chosen such that the exact solution are given by

$$\mathbf{u} = (ye^{-t}, z\cos(t), x), \quad p=0, \quad \mathbf{A} = (z, 0, y\cos(t)). \tag{4.3}$$

Note that the given exact solutions (4.3) are linear in terms of the spatial variables  $x, y, z$  which means the approximate errors are mainly due to the time discretization. We fix mesh size  $h = \frac{1}{16}$  and refine the time step size  $\delta t$ . The computational errors at  $t=1$  are shown in Fig. 1, where we observe that all errors computed by the first-order and second-order schemes show their corresponding orders of accuracy, which means the developed schemes agree with the expected theoretic optimal error rates given in (4.1) and (4.2).

## 4.2 Spatial accuracy tests

We further test the spatial convergence orders for the developed schemes. We still use the 3D computational domain  $[0,1]^3$  and parameters  $R_e = R_m = s = 1$ . The source terms and boundary conditions are chosen such that the exact solution are given as

$$\begin{cases} \mathbf{u} = (\sin(t)\sin(y), \sin(t)\sin(z), \sin(t)\sin(x)), \\ p = (2x-1)yze^{-t}, \\ \mathbf{A} = (\cos(t+z), \cos(t+x), \cos(t+y)). \end{cases} \quad (4.4)$$

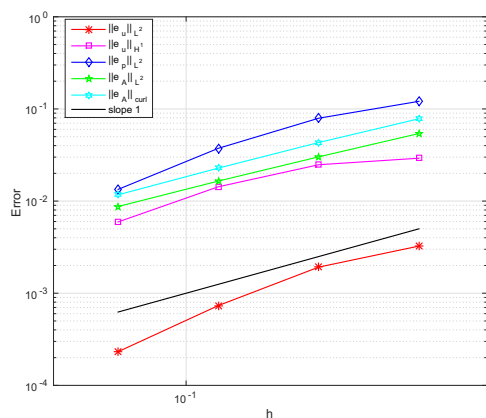
To test the spatial convergence orders of the first-order scheme (3.6)-(3.9), we set two different cases with  $\delta t = 0.5h$  and  $\delta t = h^2$ , respectively. Hence, (4.1) becomes

$$\begin{cases} \text{when } \delta t = 0.5h, & \|e_u\|_{L^2} \sim h, \|e_u\|_{H^1} \sim h, \|e_p\|_{L^2} \sim h, \|e_A\|_{L^2} \sim h, \|e_A\|_{curl} \sim h, \\ \text{when } \delta t = h^2, & \|e_u\|_{L^2} \sim h^2, \|e_u\|_{H^1} \sim h^2, \|e_p\|_{L^2} \sim h^2, \|e_A\|_{L^2} \sim h, \|e_A\|_{curl} \sim h. \end{cases}$$

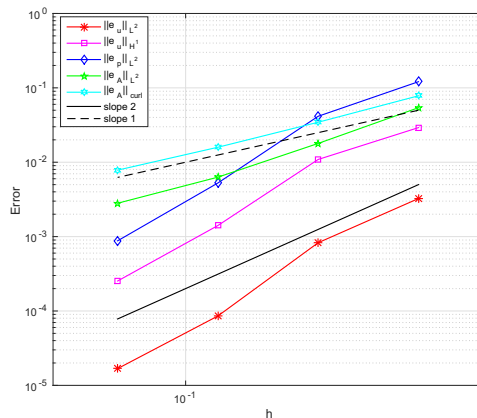
The numerical errors at  $t=1$  are plotted in Fig. 2 where we find that the  $L^2$  and  $H(curl)$  errors of potential  $\mathbf{A}$  have the asymptotic first-order accuracy. The  $L^2$  and  $H^1$  errors of velocity  $\mathbf{u}$  and the  $L^2$  error of pressure  $p$  possess a little higher order accuracy than the optimal error orders.

To verify the spatial convergence orders of the second-order schemes, we set  $\delta t = 0.25h$ , and by (4.2) there holds

$$\|e_u\|_{L^2} \sim h^2, \|e_u\|_{H^1} \sim h^2, \|e_p\|_{L^2} \sim h^2, \|e_A\|_{L^2} \sim h, \|e_A\|_{curl} \sim h.$$



(a)  $\delta t = 0.5h$ .



(b)  $\delta t = h^2$ .

Figure 2: The numerical errors for  $\|e_u\|_{L^2}$ ,  $\|e_u\|_{H^1}$ ,  $\|e_p\|_{L^2}$ ,  $\|e_A\|_{L^2}$  and  $\|e_A\|_{curl}$  at  $t=1$  computed by using the first-order scheme where (a)  $\delta t = 0.5h$ , (b)  $\delta t = h^2$  and the exact solutions are given in (4.4).

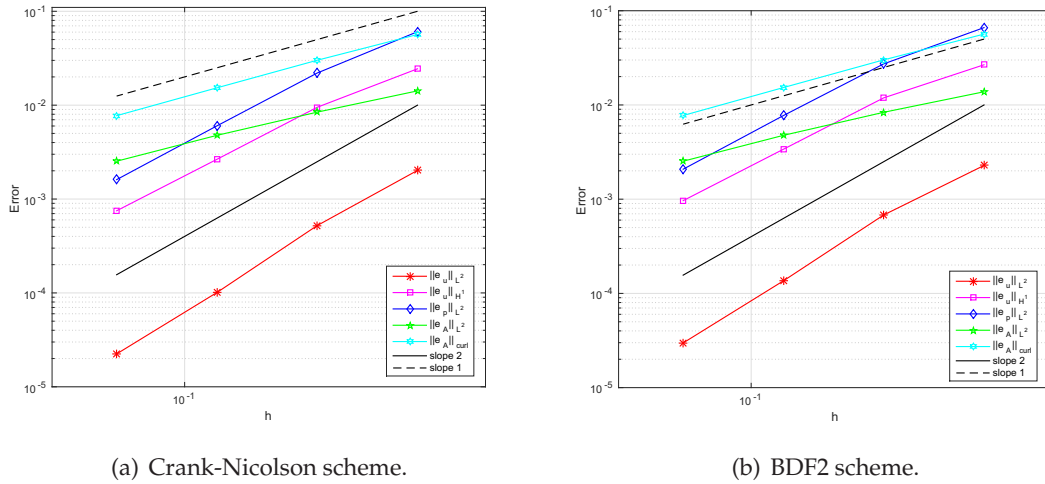


Figure 3: The numerical errors of  $\|e_u\|_{L^2}$ ,  $\|e_u\|_{H^1}$ ,  $\|e_p\|_{L^2}$ ,  $\|e_A\|_{L^2}$  and  $\|e_A\|_{curl}$  at  $t=1$  computed by using the two second-order schemes with  $\delta t = 0.25h$  where the exact solutions are given in (4.4).

The computed numerical errors at  $t = 1$  are plotted in Fig. 3, where we observe that the  $L^2$  and  $H^1$  errors of velocity  $u$  and the  $L^2$  error of pressure  $p$  possess the asymptotic second-order accuracy, and the  $L^2$  and  $H(curl)$  errors of potential  $A$  possess the first-order accuracy, as expected.

### 4.3 Energy stability tests

In this example, we verify the unconditional energy stability of the developed schemes. The 3D computed domain is still set as  $[0,1]^3$ , and the initial conditions for  $u, p, A$  are set as

$$\begin{cases} u_0 = (100x^2(x-1)^2y(y-1)(2y-1)z(z-1), -100y^2(y-1)^2x(x-1)(2x-1)z(z-1), 0), \\ p_0 = 0, \\ A_0 = (0, 100\sin(\pi x)y^2(y-1)^2z(z-1)(2z-1), -100\sin(\pi x)z^2(z-1)^2y(y-1)(2y-1)). \end{cases}$$

We set  $s = 1$ ,  $h = \frac{1}{10}$  and vary parameters  $R_e = R_m = 10, 100, 1000, 10000$ . In Figs. 4-6, we plot the time evolution of the total free energy  $E(u^n, A^n) = \frac{1}{2}\|u^n\|^2 + \frac{1}{2}s\eta\|\nabla \times A^n\|^2$  until the energy reaches steady state by using the first-order and two second-order schemes where various time step sizes  $\delta t = 0.5, 0.2, 0.1, 0.05$  are adopted. We observe that all energy curves show monotonic decays for all time step sizes which numerically confirms that our schemes are unconditionally energy stable.

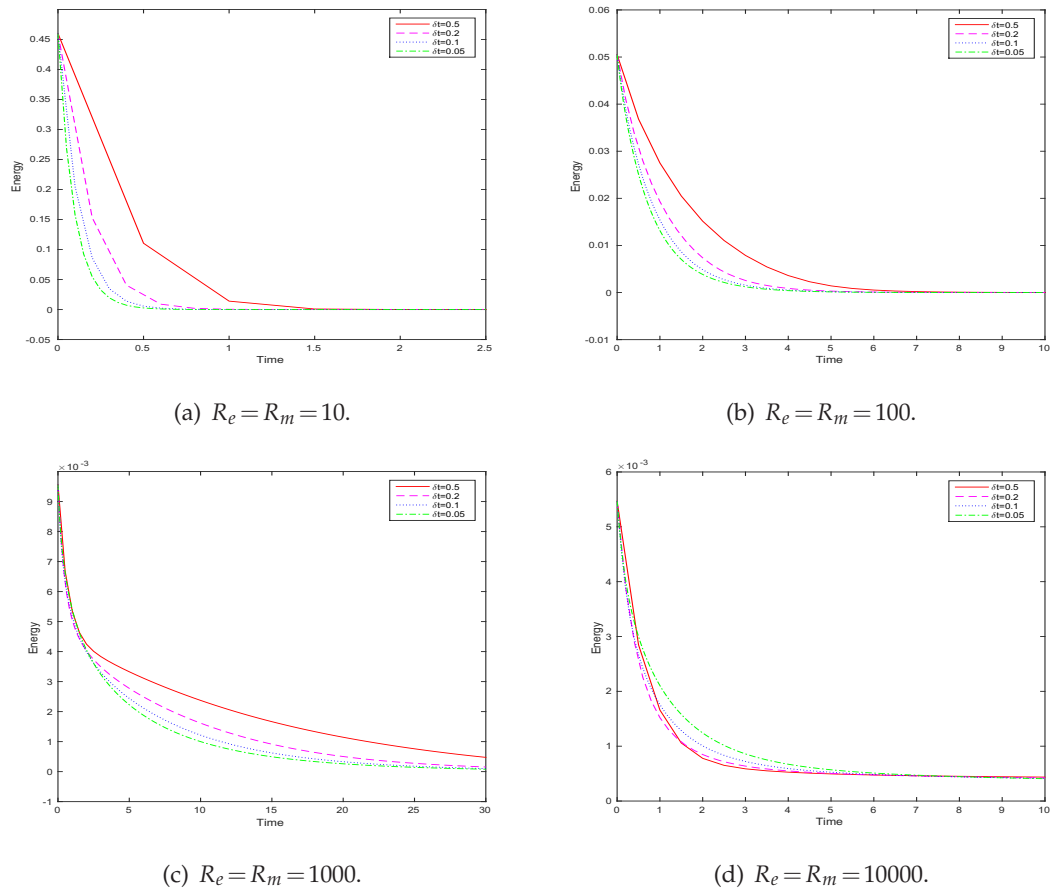


Figure 4: Time evolutions of the total free energy computed by different time step sizes until steady state where the first-order scheme is adopted.

#### 4.4 Driven cavity flow

In this example, we simulate the benchmark problem of driven cavity flow in the 3D computed domain  $[0, 1]^3$  which had been computed in [15, 24, 28, 29] using different MHD models. The initial condition of magnetic potential and velocity are given by  $A_0 = (0, 0, y)$ ,  $\mathbf{u}_0 = (v, 0, 0)$  where  $v$  is a continuous function and satisfies  $v(x, y, 1) = 1$ ,  $v(x, y, z) = 0$  as  $z \leq 1 - \epsilon$ . The top boundary ( $z = 1$ ) conditions are set by  $\mathbf{u} = \mathbf{u}_0$ , no slip boundary conditions ( $\mathbf{u} = 0$ ) are imposed on other walls. An external magnetic field effect is imposed by setting the magnetic potential boundary of  $\mathbf{A} \times \mathbf{n} = \mathbf{A}_0 \times \mathbf{n}$  on the walls.

For the relatively small Reynolds number ( $R_e < 1000$ ), the 3D hydrodynamic cavity possesses a steady-state solution. We set the time step  $\delta t = \frac{1}{100}$  and grid size  $h = \frac{1}{16}$ . We choose a relatively small Reynolds number  $R_e = 200$ ,  $s = 1$ , and investigate the effects by varying the magnetic Reynolds number  $R_m$ .

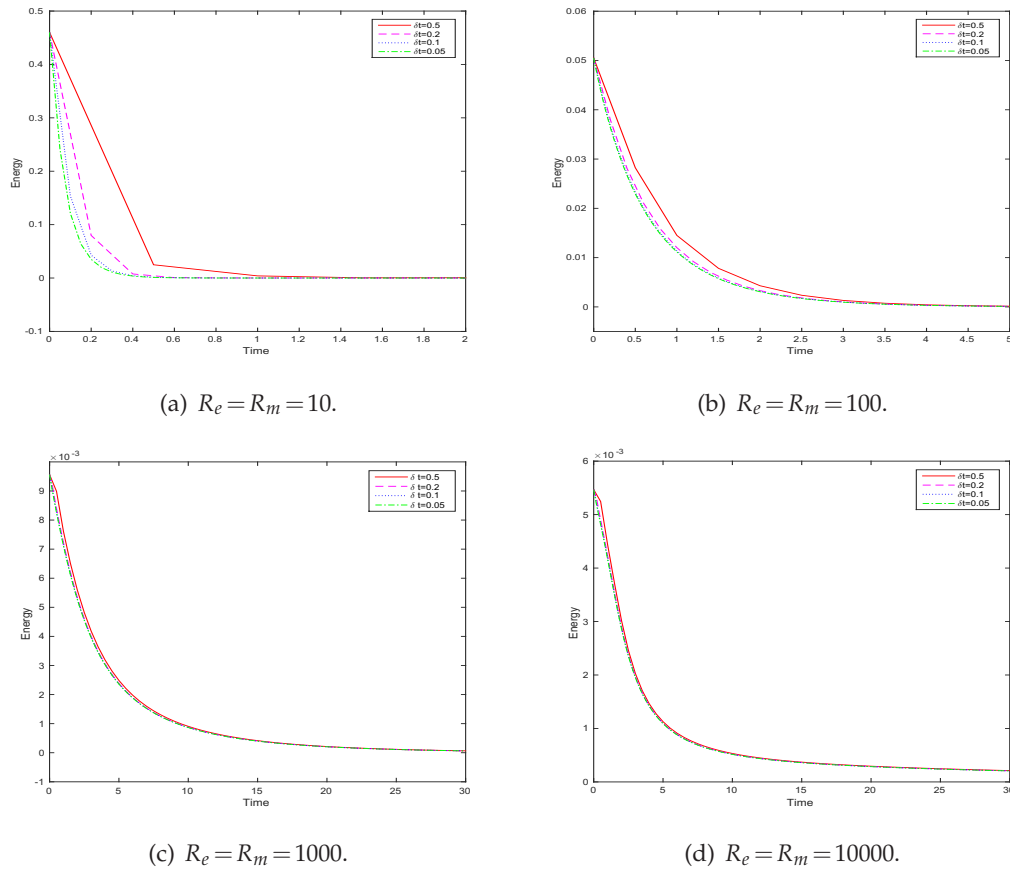


Figure 5: Time evolutions of the total free energy computed by different time step sizes until steady state where the second-order Crank-Nicolson scheme is adopted.

In Fig. 7, we depict the magnetic field  $\mathbf{B}(\mathbf{B} = \nabla \times \mathbf{A})$  for three values of  $R_m = 1, 10, 100$ . We find that, when  $R_m = 1$ , shown in Fig. 7(a), the induced magnetic field in the cavity is almost equal to the externally imposed magnetic field  $\mathbf{B}_e$  where  $\mathbf{B}_e = \nabla \times \mathbf{A}_0 = (1, 0, 0)$ . When  $R_m$  increases, for example,  $R_m = 100$  shown in Fig. 7(c), the strength of the induced magnetic field in the cavity is enhanced and a vortex in the magnetic field appears. In Fig. 8, we plot the 2D cut-off planes of the streamlines of the velocity field at  $y = 0.5$ . We observe that a small eddy at the bottom cavity gradually weakens as the magnetic Reynolds number  $R_m$  increases.

#### 4.5 Hydromagnetic Kelvin-Helmholtz instability

In this example, we perform numerical simulations for the benchmark problem of Kelvin-Helmholtz instability caused by a shear-layer flow, cf. [4, 6, 7, 11, 12, 16, 29, 31] and the references therein.

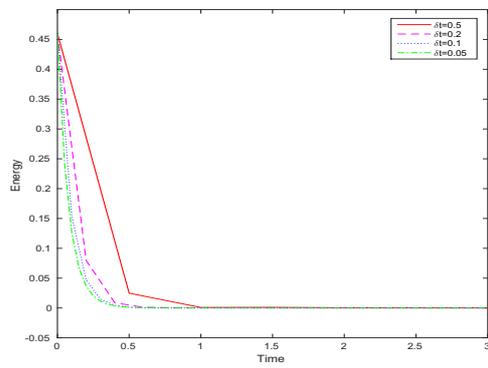
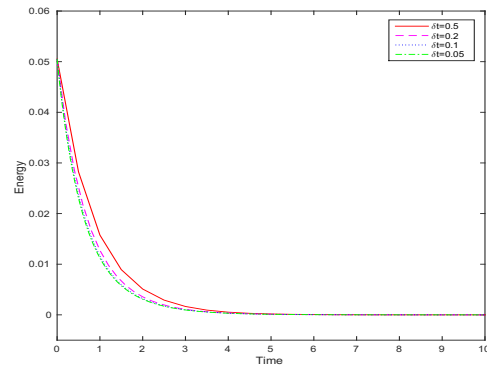
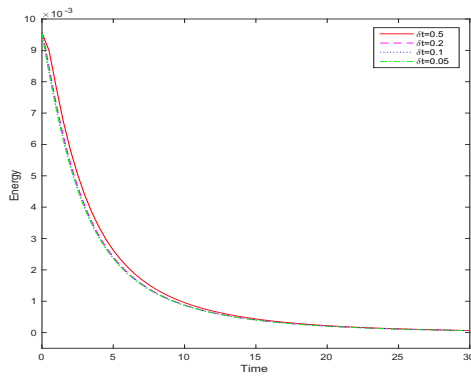
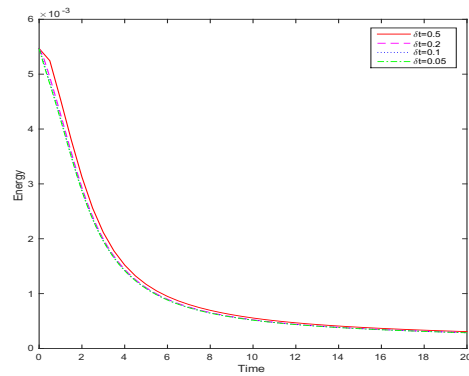
(a)  $R_e = R_m = 10$ .(b)  $R_e = R_m = 100$ .(c)  $R_e = R_m = 1000$ .(d)  $R_e = R_m = 10000$ .

Figure 6: Time evolutions of the total free energy computed by different time step sizes until steady state where the second-order BDF2 scheme is adopted.

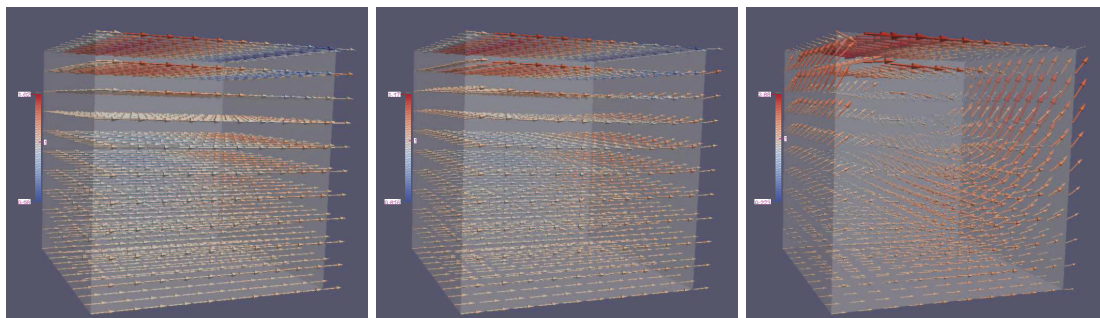
(a)  $R_m = 1$ .(b)  $R_m = 10$ .(c)  $R_m = 100$ .

Figure 7: Driven cavity example: the magnetic field  $B$  computed by using three magnetic Reynolds numbers  $R_m = 1, 10, 100$ .

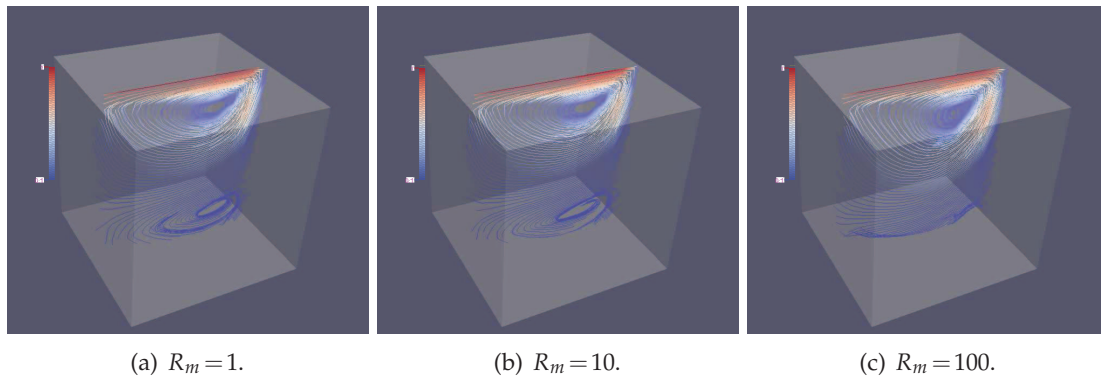


Figure 8: Driven cavity example: the streamlines of velocity field at the cut-off plane of  $y = 0.5$  with  $R_m = 1, 10, 100$ .

We set the computed domain as  $\Omega = [0, 2] \times [0, 1] \times [0, 1]$  and initialize the velocity profile as  $\mathbf{u}_0 = (1.5, 0, 0)$  in the domain of  $z \geq 0.5$ ,  $\mathbf{u}_0 = (-1.5, 0, 0)$  in the domain of  $z \leq 0.5$ . The initial profile of the magnetic potential is set as  $\mathbf{A}_0 = (0, 0, -\delta \ln(\cosh(x/\delta)))$ , where  $\delta = 0.07957747154595$  [7]. A sheared external magnetic field is imposed through the boundary conditions for the magnetic potential  $\mathbf{A}$  that are set as  $\mathbf{A} \times \mathbf{n} = \mathbf{A}_0 \times \mathbf{n}$  for the top wall of  $z = 1$  and  $-\mathbf{A}_0 \times \mathbf{n}$  for the bottom wall of  $z = 0$ . At the left and right walls of  $x = 0$  and  $x = 2$ , periodic boundary conditions are applied on the magnetic potential  $\mathbf{A}$  and velocity  $\mathbf{u}$ . No slip boundary conditions of the second and third components of velocity  $\mathbf{u} = (u_1, u_2, u_3)$  are imposed on the top ( $z = 1$ ) and bottom walls ( $z = 0$ ), i.e.,  $u_2 = u_3 = 0$ . No slip boundary conditions of the second component  $u_2$  are also set at the back ( $y = 0$ ) and front walls ( $y = 1$ ). We choose the parameters  $R_e = R_m = 1000$ ,  $s = 0.1$ , and use  $\delta t = \frac{1}{100}$ ,  $h = \frac{1}{16}$  to discretize the time and space.

In Figs. 9-10, we show snapshots of the velocity field  $\mathbf{u}$  and streamlines of  $\mathbf{u}$  at the plane of  $y = 0.5$  at the moment  $t = 0.01, 0.1, 0.2, 0.35, 0.5, 0.75, 1.0, 2.0$ . When time evolves, we observe several vortices appear in the domain and they deform and rotate along with the flow field. The profiles of vortices and the magnetic field show the typical structure of K-H instability which coincide well with the numerical/experimental results discussed in [4, 6, 16, 31], qualitatively.

## 5 Concluding remarks

In this paper, we develop several efficient linear, decoupled and unconditionally energy stable schemes for solving the potential MHD model. We establish the well-posedness of the schemes and prove their unconditional energy stabilities rigorously. A series of numerical experiments, including benchmark problems of driven cavity flow and Kelvin-Helmholtz instability, are implemented to demonstrate the stability and the accuracy of the schemes.

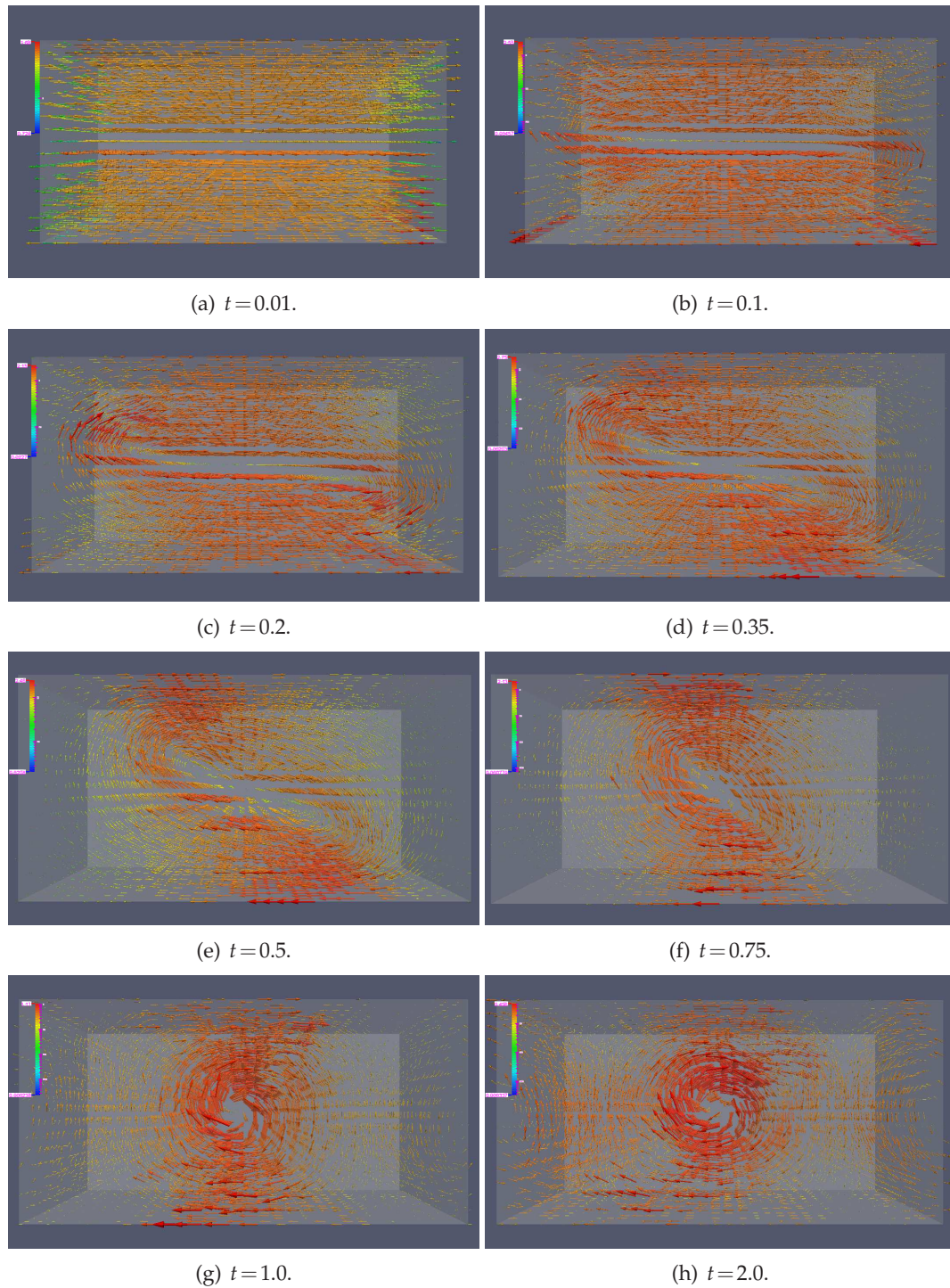


Figure 9: K-H instability example: snapshots of the velocity field are taken at  $t=0.01, 0.1, 0.2, 0.35, 0.5, 0.75, 1.0, 2.0$ .

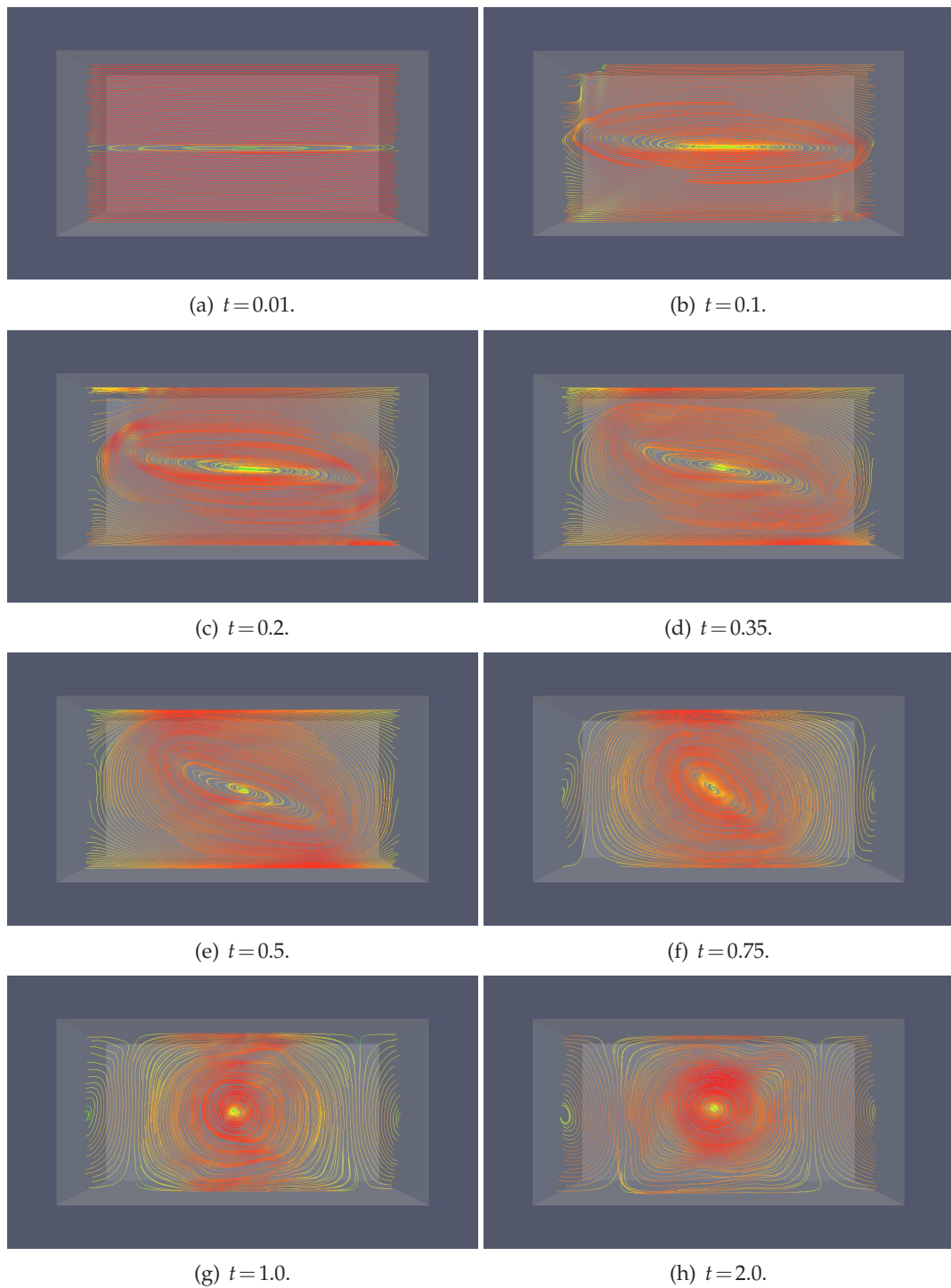


Figure 10: K-H instability example: snapshots of the stream lines of velocity field are taken at various times where  $y=0.5$ .

## Acknowledgments

The research of G.-D. Zhang is partially supported by National Science Foundation of China under grant numbers 11601468 and 11771375, and Shandong Province Natural Science Foundation (ZR2018MA008). The research of X. Yang is partially supported by the U.S. National Science Foundation under grant numbers DMS-1720212, DMS-1818783, and DMS-2012490.

## References

- [1] J. H. Adler, T. R. Benson, E. C. Cyr, S. P. MacLachlan, and R. S. Tuminaro. Monolithic multi-grid methods for two-dimensional resistive magnetohydrodynamics. *SIAM J. Sci. Comput.*, 38(1):B1–B24, 2016.
- [2] S. H. Aydın, A. Neslitürk, and M. Tezer-Sezgin. Two-level finite element method with a stabilizing subgrid for the incompressible MHD equations. *International Journal for Numerical Methods in Fluids*, 62(2):188–210, 2010.
- [3] S. Badia, R. Planas, and J. V. Gutiérrez-Santacreu. Unconditionally stable operator splitting algorithms for the incompressible magnetohydrodynamics system discretized by a stabilized finite element formulation based on projections. *International Journal for Numerical Methods in Engineering*, 93(3):302–328, 2013.
- [4] H. Baty, R. Keppens, and P. Comte. The two-dimensional magnetohydrodynamic kelvin-helmholtz instability: compressibility and large-scale coalescence effects. *Phys. of Plasmas*, 10:4661–4674, 2003.
- [5] J. U. Brackbill and D. C. Barnes. The effect of nonzero  $\nabla \cdot \mathbf{B}$  on the numerical solution of the magnetohydrodynamic equations1. *Journal of Computational Physics*, 35(3):426–430, 1980.
- [6] S. R. Choudhury. The initial-value problem for the kevin-helmholtz instability of high velocity and magnetized shear layers. *Qual. Appl. Math.*, LIV:637–662, 1996.
- [7] E. C. Cyr, J. N. Shadid, R. S. Tuminaro, R. P. Pawlowski, and L. Chacón. A new approximate block factorization preconditioner for two-dimensional incompressible (reduced) resistive MHD. *SIAM Journal on Scientific Computing*, 35(3):B701–B730, 2013.
- [8] W. Dai and P. R. Woodward. On the divergence-free condition and conservation laws in numerical simulations for supersonic magnetohydrodynamical flows. *Astrophysical Journal*, 494(1), 1998.
- [9] J.-F. Gerbeau, C. Le Bris, and T. Lelièvre. *Mathematical Methods for the Magnetohydrodynamics of Liquid Metals*. Clarendon Press, 2006.
- [10] V. Girault and P.A. Raviart. Finite Element Method for Navier-Stokes Equations: Theory and Algorithms. *Springer-Verlag, Berlin, Heidelberg*, pages 395–414, 1987.
- [11] J. P. Goedbloed, R. Keppens, and S. Poedts. *Advanced Magnetohydrodynamics: With Applications to Laboratory and Astrophysical Plasmas*. Cambridge University Press, 2010.
- [12] J. P. Hans Goedbloed and S. Poedts. *Principles of Magnetohydrodynamics with Applications to Laboratory and Astrophysical Plasmas*. Cambridge University Press, 2004.
- [13] M. D. Gunzburger, A. J. Meir, and J. S. Peterson. On the existence, uniqueness, and finite element approximation of solutions of the equations of stationary, incompressible magnetohydrodynamics. *Mathematics of Computation*, 56(194):523–563, 1991.
- [14] Y. He. Unconditional convergence of the Euler semi-implicit scheme for the three-dimensional incompressible MHD equations. *IMA J. Num. Anal.*, 35(2):767–801, 2014.

- [15] R. Hiptmair, L. Li, S. Mao, and W. Zheng. A fully divergence-free finite element method for magnetohydrodynamic equations. *Mathematical Models and Methods in Applied Sciences*, 28(04):659–695, 2018.
- [16] T. W. Jones, J. B. Gaalaas, D. Ryuand, and A. Frank. The MHD Kelvin-Helmholtz instability. II. The roles of weak and oblique fields in planar flows. *The Astrophysical J.*, pages 230–244, 1997.
- [17] W. Layton, H. Tran, and C. Trenclea. Numerical analysis of two partitioned methods for uncoupling evolutionary MHD flows. *Numerical Methods for Partial Differential Equations*, 30(4):1083–1102, 2014.
- [18] F. Lin, L. Xu, and P. Zhang. Global small solutions of 2-D incompressible MHD system. *J. Diff. Eqns.*, 259(10):5440–5485, 2015.
- [19] F. Lin and P. Zhang. Global small solutions to an MHD-type system: The three-dimensional case. *Comm. on Pure and Appl. Math.*, 67(4):531–580, 2014.
- [20] C. Liu, J. Shen, and X. Yang. Decoupled energy stable schemes for a phase-field model of two-phase incompressible flows with variable density. *J. Sci. Comput.*, 62:601–622, 2015.
- [21] J.-G. Liu and R. Pego. Stable discretization of magnetohydrodynamics in bounded domains. *Comm. in Math. Sci.*, 8(1):235–251, 2010.
- [22] Y. Liu, Q. Liu, Y. Liu, C.-W. Shu, and M. Zhang. Locally divergence-free spectral-DG methods for ideal magnetohydrodynamic equations on cylindrical coordinates. *Communications in Computational Physics*, 26(3):631–653, 2019.
- [23] A. Logg, K. A. Mardal, and G.N. Wells. *Automated Solution of Differential Equations by the Finite Element Method*. Springer, 2012.
- [24] Y. Ma, K. Hu, X. Hu, and J. Xu. Robust preconditioners for incompressible MHD models. *J. Comput. Phys.*, 316:721–746, 2016.
- [25] P. Monk. *Finite Element Methods for Maxwell's Equations*. Oxford University Press, 2003.
- [26] R. J. Moreau. *Magnetohydrodynamics*, volume 3. Springer Science & Business Media, 2013.
- [27] J. C. Nédélec. A new family of mixed finite elements in  $\mathbb{R}^3$ . *Numerische Mathematik*, 50(1):57–81, Jan 1986.
- [28] E. G. Phillips, H. C. Elman, Eric C Cyr, J. N. Shadid, and R. P. Pawlowski. A block preconditioner for an exact penalty formulation for stationary MHD. *SIAM Journal on Scientific Computing*, 36(6):B930–B951, 2014.
- [29] E. G. Phillips, J. N. Shadid, E. C. Cyr, H. C. Elman, and R. P. Pawlowski. Block preconditioners for stable mixed nodal and edge finite element representations of incompressible resistive MHD. *SIAM J. Sci. Comput.*, 38(6):B1009–B1031, 2016.
- [30] E. R. Priest and A. W. Hood. *Advances in Solar System Magnetohydrodynamics*. Cambridge University Press, 1991.
- [31] D. Ryu, T. W. Jones, and A. Frank. The magnetohydrodynamic Kelvin-Helmholtz instability: A three-dimensional study of nonlinear evolution. *The Astrophysical J.*, 545:475–493, 2000.
- [32] N. B. Salah, A. Soulaïmani, and W. G. Habashi. A finite element method for magnetohydrodynamics. *Comp. Meth. in Appl. Mech. Eng.*, 190(43):5867–5892, 2001.
- [33] M. Sermange and R. Temam. Some mathematical questions related to the MHD equations. *Comm. on Pure and Appl. Math.*, 36(5):635–664, 1983.
- [34] J. Shen and X. Yang. Decoupled energy stable schemes for phase field models of two phase complex fluids. *SIAM J. Sci. Comput.*, 36:B122–B145, 2014.
- [35] J. Shen and X. Yang. Decoupled, energy stable schemes for phase-field models of two-phase incompressible flows. *SIAM J. Numer. Anal.*, 53(1):279–296, 2015.
- [36] J. Shen, X. Yang, and H. Yu. Efficient energy stable numerical schemes for a phase field

- moving contact line model. *J. Comput. Phys.*, 284:617–630, 2015.
- [37] R. Temam. Sur l'approximation de la solution des équations de Navier-Stokes par la méthode des pas fractionnaires II. *Arch. Rat. Mech. Anal.*, 33:377–385, 1969.
- [38] G. Tóth. The  $\nabla \cdot \mathbf{B} = 0$  constraint in shock-capturing magnetohydrodynamics codes. *Journal of Computational Physics*, 161(2):605–652, 2000.
- [39] G.-D. Zhang and C. Chen. Uniformly robust preconditioners for incompressible MHD system. *Journal of Computational and Applied Mathematics*, page 112914, 2020.